NASA/TM—2018-218874

Acoustic Methods Used in the NASA Glenn 9- by 15-Foot Low-Speed Wind Tunnel

Clifford A. Brown and David B. Stephens
Glenn Research Center, Cleveland, Ohio

June 2018

NASA STI Program . . . in Profile

Since its founding, NASA has been dedicated to the advancement of aeronautics and space science. The NASA Scientific and Technical Information (STI) Program plays a key part in helping NASA maintain this important role.

The NASA STI Program operates under the auspices of the Agency Chief Information Officer. It collects, organizes, provides for archiving, and disseminates NASA's STI. The NASA STI Program provides access to the NASA Technical Report Server—Registered (NTRS Reg) and NASA Technical Report Server—Public (NTRS) thus providing one of the largest collections of aeronautical and space science STI in the world. Results are published in both non-NASA channels and by NASA in the NASA STI Report Series, which includes the following report types:

- TECHNICAL PUBLICATION. Reports of completed research or a major significant phase of research that present the results of NASA programs and include extensive data or theoretical analysis. Includes compilations of significant scientific and technical data and information deemed to be of continuing reference value. NASA counter-part of peer-reviewed formal professional papers, but has less stringent limitations on manuscript length and extent of graphic presentations.

- TECHNICAL MEMORANDUM. Scientific and technical findings that are preliminary or of specialized interest, e.g., "quick-release" reports, working papers, and bibliographies that contain minimal annotation. Does not contain extensive analysis.

- CONTRACTOR REPORT. Scientific and technical findings by NASA-sponsored contractors and grantees.

- CONFERENCE PUBLICATION. Collected papers from scientific and technical conferences, symposia, seminars, or other meetings sponsored or co-sponsored by NASA.

- SPECIAL PUBLICATION. Scientific, technical, or historical information from NASA programs, projects, and missions, often concerned with subjects having substantial public interest.

- TECHNICAL TRANSLATION. English-language translations of foreign scientific and technical material pertinent to NASA's mission.

For more information about the NASA STI program, see the following:

- Access the NASA STI program home page at http://www.sti.nasa.gov

- E-mail your question to help@sti.nasa.gov

- Fax your question to the NASA STI Information Desk at 757-864-6500

- Telephone the NASA STI Information Desk at 757-864-9658

- Write to:
  NASA STI Program
  Mail Stop 148
  NASA Langley Research Center
  Hampton, VA 23681-2199

NASA/TM—2018-218874

Acoustic Methods Used in the NASA Glenn 9- by 15-Foot Low-Speed Wind Tunnel

Clifford A. Brown and David B. Stephens
Glenn Research Center, Cleveland, Ohio

National Aeronautics and
Space Administration

Glenn Research Center
Cleveland, Ohio 44135

June 2018

Acknowledgments

This report was funded by the NASA Advanced Air Transport Technology Project. Dr. Edmane Envia in the NASA Glenn Research Center Acoustics Branch derived the sound power calculation described in Section 3.2. Gary Podboy and Dave Elliott, also from the NASA Glenn Research Center Acoustics Branch, served as technical reviewers for this work.

This work was sponsored by the Advanced Air Vehicle Program at the NASA Glenn Research Center

Level of Review: This material has been technically reviewed by technical management.

Available from

NASA STI Program
Mail Stop 148
NASA Langley Research Center
Hampton, VA 23681-2199

National Technical Information Service
5285 Port Royal Road
Springfield, VA 22161
703-605-6000

This report is available in electronic form at http://www.sti.nasa.gov/ and http://ntrs.nasa.gov/

Acoustic Methods Used in the NASA Glenn 9- by 15-Foot Low-Speed Wind Tunnel

Clifford A. Brown and David B. Stephens
National Aeronautics and Space Administration
Glenn Research Center
Cleveland, Ohio 44135

Abstract

The 9- by 15-Foot Low Speed Wind Tunnel has been used for acoustic testing for more than 40 years. The facility is principally used for testing aircraft engine propulsion components, for both aerodynamic performance and acoustics. The present report discusses the instrumentation and procedures currently used for the acquisition of high-quality acoustic data from aircraft engine fan models.

Nomenclature

ϕ	azimuthal angle in tunnel coordinate system
θ	polar angle in tunnel coordinate system
θ_e	angle of sound emission
θ_g	geometric angle from noise source to microphone
θ_i	angle of sound incidence on microphone
$_{AMF}$	Subscript, microphone forebody correction
$_{FR}$	Subscript, microphone frequency response correction
f	Frequency, Hz
G	Auto-power spectral density, dB/Hz
H	Transfer function or gain factor, dB

1 Introduction

The 9- by 15-foot (cross-section) Low Speed Wind Tunnel (9x15 LSWT) was originally designed to test the aerodynamic performance of vertical/short take-off and landing (V/STOL) aircraft models at the NASA Glenn Research Center (GRC). Sound-absorbing deep acoustic panels were installed in the test section in 1986; since then the 9x15 LSWT has been principally used to test the noise and performance of aircraft propulsion systems.

The 9x15 LSWT was built inside the return leg of the 8- by 6-foot (cross-section) Supersonic Wind Tunnel (8x6 SWT).[1] The 8x6 SWT, completed in 1949, was designed as an open-exhaust tunnel to test fuel-burning ramjet engines. A large muffler section was added downstream of the test section in 1950 to mitigate community noise issues[2]. The 9x15 LSWT was built in 1968 to create the 8x6/9x15 Wind Tunnel Complex (Figure 1). Air is driven through the circuit by a 7-stage axial compressor powered by 3 electric motors that together generate up to 65 MW (87,000 HP). A set of doors allow the tunnel to run in a fully-closed or partially-open configuration, introducing some outside air, depending on the test requirements.

A desiccant dryer bed reduces the humidity in the tunnel. A number of reports overview the facility's aerodynamic test capabilities[3, 4, 5] and acoustic quality[6, 7, 8, 9].

The 9x15 has been used to test model turbofans and propellers for both NASA research projects and external customers.[10, 11, 12] Turbofan models are powered by the NASA Ultra-High Bypass drive rig[13] while a counter-rotating drive rig is used for open rotor testing[14]. A typical fan model undergoing acoustic testing in the 9x15 LSWT is shown in Figure 2.

Many modern automotive and aerospace acoustic tunnels are of open-jet or 3/4-configuration (top and side-walls removed)[15]. In contrast, the 9x15 LSWT is a closed-wall tunnel. There are advantages and disadvantages to each configuration depending on the model type and data collected. Fan models in the 9x15 LSWT are frequently run at an angle-of-attack relative to the incoming flow to simulate take-off, landing, or cross-wind situations. These orientations would likely disrupt the flow into the collector of an open-jet or 3/4-configuration tunnel creating a new noise source. While closed-wall tunnels do not require a flow collector, they generally have higher background (no model) noise levels due to the tunnel flow over the test section walls. In addition, the microphones must be located in the tunnel flow which increases the noise floor (microphone self-noise). The microphones are typically placed outside the flow in an open-jet or 3/4-configuration to reduce the self-noise but the sound waves must then propagate through a shear-layer where they can be redirected and distorted. Tonal noise, produced by the rotating machinery commonly tested in the 9x15 LSWT, can be particularly affected by passing through a shear-layer.[1]

This report documents the instrumentation and data processing commonly used in the 9x15 LSWT for acoustic testing. Section 2 describes the in-flow traversing microphone system and related data processing corrections. Section 3 describes the data processing methods used to calculate common noise metrics such as sound power and effective perceived noise level (EPNL). Finally, Section 4 describes other acoustic measurement systems that have been used but are less commonly deployed.

2 In-Flow Traversing Microphone System

In-flow microphone measurements made in the 9x15 LSWT are conducted according to the recommendations given in Chapter 1 of *Aeroacoustic Measurements*[16]. This section discusses the data acquisition and processing methods, the typical microphone layout, and the calibration of microphone windscreens used to make in-flow noise measurements in the 9x15 LSWT.

2.1 Tunnel Layout

The 9x15 LWST test section, configured for in-flow traversing microphone measurements, is shown in Figure 3. All traversing microphone stops are described relative to the acoustic origin which is defined at the center of the fan stacking axis. Then, by historical convention, the aircraft roll axis (x-axis) is positive in the direction of flight, the aircraft pitch axis (y-axis) is positive in the direction toward the microphones, and the aircraft yaw axis (z-axis) is positive toward the floor[2]. Note that the coordinate system does not rotate with the model at angle of attack orientations, although the coordinate system does translate with the movement of the model.

The primary acoustic instrumentation is a three-microphone traversing probe located on a 2.26 m (89 inches) sideline from the acoustic origin (Figure 2, left side). The 6.6-m (260-inch) long traverse mechanism can move the microphone between polar angles $27^\circ \leq \theta \leq 135^\circ$ as measured from the upstream flight (roll) axis. The height of the fan model above the tunnel floor (z=0) is defined by the drive rig and, therefore, consistent between models; the traverse microphones are located at azimuthal angles $\phi = 0$ and $\phi = \pm 22.5^\circ$. Three fixed microphones, located at $\theta \approx 140^\circ$, $\theta \approx 150^\circ$, and $\theta \approx 160^\circ$, are used to fill in the aft angles that the traverse does not reach (shown to the left of the drive rig in Figure 2). Other fixed microphones can be added to accommodate specific test requirements.

[1] A turbulent shear-layer will tend to distort a pure tone spreading the energy over a small but signifiant frequency range. This may effect the peak amplitude and frequency of the tone depending on the severity of the distortion (turbulence intensity in the shear-layer) and data processing techniques used (e.g. FFT window size).

[2] The yaw axis is positive toward the floor for consistency between new and past datasets. Only one microphone was used on the traverse, at the model centerline (z=0), until 2013. When the additional top and bottom traverse microphones were added, a right-hard coordinate system consistent with the previous data required positive z-axis to be toward the floor.

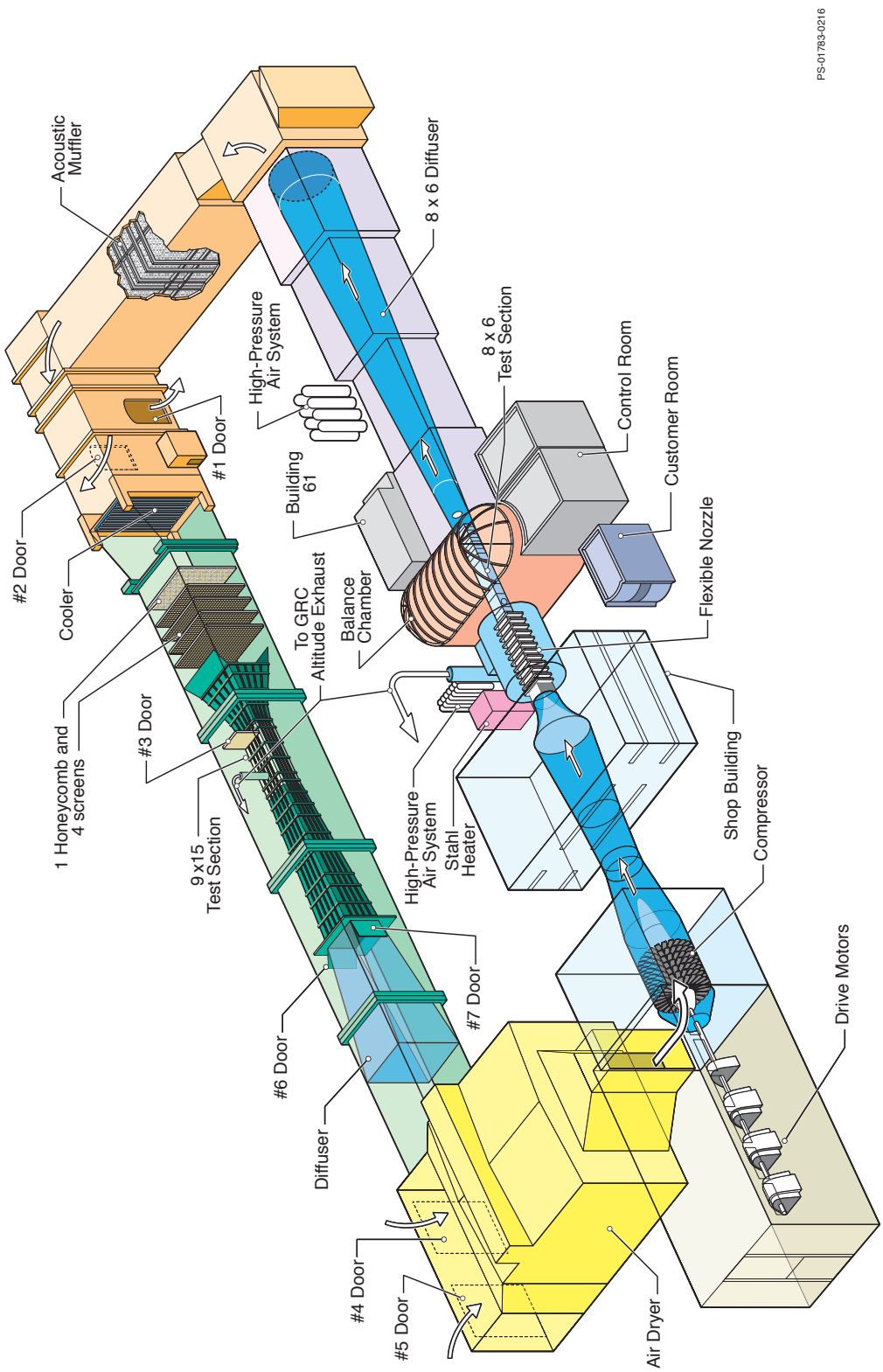

Figure 1: Schematic of the 8x6/9x15 Wind Tunnel Complex.

Figure 2: Example of a typical fan test in 9x15. A gray traversing probe holder with three microphones is shown on the far left of the image. Three fixed microphones are mounted to white probe holders between the traverse track and the fan rig strut. Upstream microphones mounted to floor and ceiling in front of fan. NASA GRC Image C-2014-8260.

2.2 Instrumentation and Data Systems

Standard acoustic instrumentation consists of Brüel and Kjær Type 4939 6.35 mm (1/4-inch) free-field microphones equipped with windscreens as described in Section 2.5. A mix of Falcon Range Type 2670 6.35 mm (1/4-inch) and Larson-Davis PRM902 0240 12.7 mm (1/2-inch, with Brüel and Kjær UA-0035 12.7 mm (1/2-inch) to 6.35 mm (1/4-inch) adapter) microphone pre-amplifiers are used. Brüel and Kjær Nexus units provide signal conditioning and amplification (in 10 dB increments). Data are digitized and recorded by a DataMAX Instrumentation Recorder from R.C. Electronics. The DataMAX uses 16-bit analog-to-digital converters to digitize the incoming signal with a 200 kHz sample rate and a 90 kHz anti-aliasing filter. Fan shaft once-per-revolution and sixty-per-revolution signals are acquired simultaneously with the microphone signals using the same DataMAX recorder.

2.3 Fixed-Stop Traversing Microphone System

An in-flow microphone can not be placed directly downstream of another in-flow microphone (or any object also in the flow); the turbulent wake from the upstream microphone will interact with the downstream microphone effectively increasing the background noise (via the microphone self-noise mechanism). There are two methods used to overcome this challenge: offset the microphones in the radial or azimuthal directions so the wakes will not interact with the downstream microphones or use a traversing system so there are no microphones downstream of the measuring array. Since the confined space of the 9x15 LSWT makes offsetting a large microphone array impractical, a traversing microphone system is used.

The 9x15 LSWT traversing microphone moves on a line parallel to the direction of flow as shown in Figure 3). Measurement locations, or stops, are pre-programmed into the traverse control computer along with a dwell time at each stop (movement settling time plus data acquisition time); this allows the measurement locations to be tailored to the specific test requirements. The standard traverse location is at 89-inches from the model origin. A typical traverse contains 48-stops set at even $\theta = 2.5°$ polar angle increments (Table 1) with a 15-second dwell time (10 seconds data acquisition plus 5 seconds settling time). One of these 48-stop surveys requires about 15 minutes to complete.

Time series data are acquired for 10 seconds at each traverse stop and processed exactly like a fixed microphone, using a 2^{14} point Hanning window function with 50% window overlap to yield a 12.21 Hz spectral bandwidth. Windows with clipped (over-range) data are removed and the remaining windows ensemble averaged (192 windows averaged if all window blocks are valid).

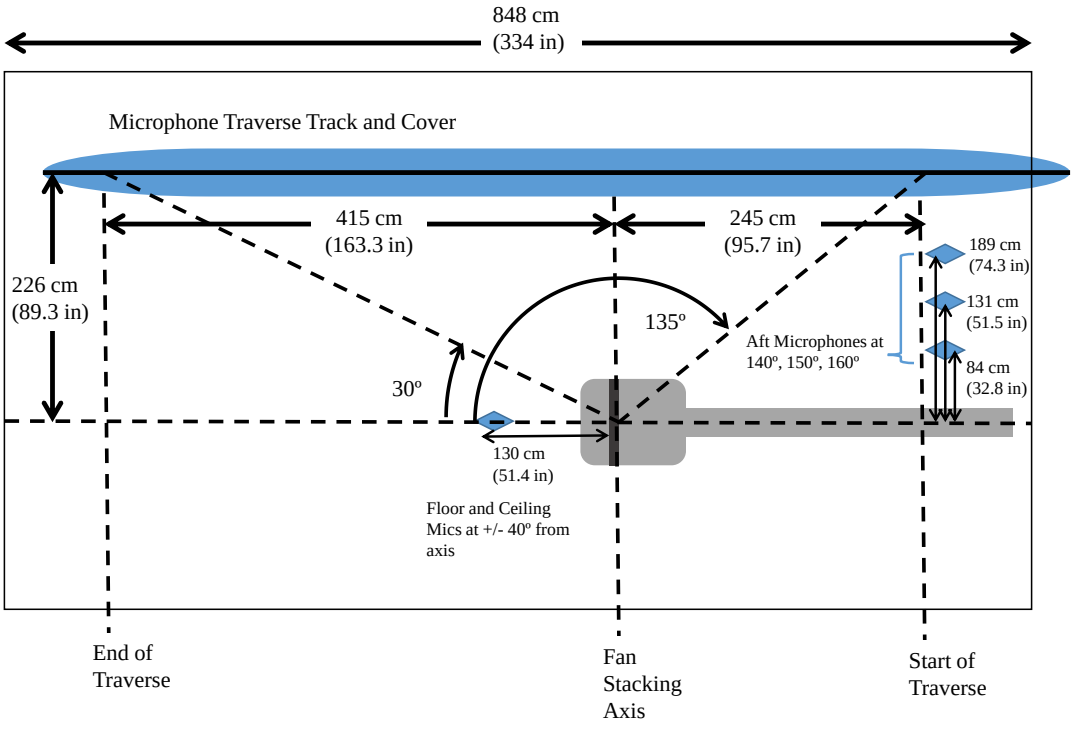

Figure 3: Schematic of a typical microphone layout used for a fan rig test in the 9x15 LSWT.

2.4 Continuous Scan Measurements

An alternate method of operating the traverse is continuous scan. Instead of stepping the traverse through a series of pre-programmed locations, with a settling and dwell time at each location, the traverse is moved continuously along the track while data are acquired. A Temposonics linear-position sensor, installed alongside the screw-drive in the traversing mechanism, measures the position of the microphone as a function of time; the position signal is digitized and recored simultaneously with the acoustic data using the same data recorder so that the precise location of the microphone is always known. These data can be processed using a simple method, e.g. computing a Fourier transform using data centered on a location, or using more complex order-tracking methods[17]. A continuous traverse acquisition in the 9x15 LSWT takes approximately 4.5

Table 1: Microphone measurement angles for a typical fan test.

Traverse Stop Number	*Microphone Position Number*	*Distance from Aft Location (inches)*	*Geometric Angle*	*Emitted Angle at Mach 0.10*	*Emitted Angle at Mach 0.15*	*Emitted Angle at Mach 0.20*
	1		160.0	158.0	157.1	156.1
	2		150.0	147.1	145.7	144.3
	3		140.0	136.3	134.5	132.6
1	4	0.0	134.6	130.5	128.5	126.4
2	5	6.7	132.3	128.1	125.9	123.8
3	6	13.0	130.0	125.6	123.4	121.2
4	7	18.9	127.7	123.2	120.9	118.6
5	8	24.4	125.4	120.7	118.4	116.0
6	9	29.6	123.1	118.3	115.9	113.5
7	10	34.5	120.8	115.9	113.4	110.9
8	11	39.2	118.5	113.5	110.9	108.4
9	12	43.7	116.2	111.1	108.5	105.9
10	13	48.0	114.0	108.8	106.1	103.5
11	14	52.2	111.7	106.4	103.7	101.0
12	15	56.2	109.4	104.0	101.3	98.5
13	16	60.2	107.1	101.6	98.9	96.1
14	17	64.0	104.8	99.3	96.5	93.7
15	18	67.8	102.5	96.9	94.1	91.2
16	19	71.5	100.2	94.6	91.7	88.8
17	20	75.1	97.9	92.2	89.4	86.5
18	21	78.7	95.7	90.0	87.1	84.2
19	22	82.3	93.4	87.7	84.8	81.9
20	23	85.8	91.1	85.4	82.5	79.6
21	24	89.4	88.8	83.1	80.2	77.3
22	25	92.9	86.5	80.8	77.9	75.0
23	26	96.5	84.2	78.5	75.6	72.7
24	27	100.1	81.9	76.2	73.4	70.5
25	28	103.7	79.6	74.0	71.1	68.3
26	29	107.4	77.4	71.8	69.0	66.1
27	30	111.2	75.1	69.6	66.8	64.0
28	31	115.0	72.8	67.3	64.6	61.8
29	32	119.0	70.5	65.1	62.4	59.6
30	33	123.0	68.2	62.9	60.2	57.5
31	34	127.2	65.9	60.7	58.0	55.4
32	35	131.5	63.6	58.5	55.9	53.3
33	36	136.0	61.3	56.3	53.7	51.2
34	37	140.7	59.1	54.2	51.7	49.2
35	38	145.7	56.8	52.0	49.6	47.2
36	39	150.9	54.5	49.8	47.5	45.1
37	40	156.4	52.2	47.7	45.4	43.1
38	41	162.3	49.9	45.5	43.3	41.1
39	42	168.5	47.6	43.4	41.2	39.1
40	43	175.3	45.3	41.2	39.2	37.1
41	44	182.6	43.0	39.1	37.1	35.2
42	45	190.6	40.7	37.0	35.1	33.2
43	46	199.3	38.5	34.9	33.1	31.3
44	47	209.0	36.2	32.8	31.1	29.4
45	48	219.8	33.9	30.7	29.1	27.5
46	49	231.9	31.6	28.6	27.1	25.6
47	50	245.7	29.3	26.5	25.1	23.7
48	51	260.0	27.2	24.6	23.3	22.0

minutes at 1-inch/second travel speed[3].

The continuous scan measurement technique has two significant advantages over fixed-stop system: (1) a large reduction in data acquisition time and (2) the ability to extract spectra at any polar angle along the traverse track. However, processing continuous scan requires a trade-off between temporal and spatial resolution. For a given time series record, using a longer time window gives more ensemble averages while the microphone covers a wider range of angles reducing spatial resolution. Conversely, using a shorter time window keeps the microphone close to the desired angle but gives fewer ensemble averages. Figure 4 compares the directivity produced by a fan model as measured using continuous scan and fixed-stop scan[4]. The continuous scan data were processed using a short-time Fourier transform method at $\theta = 0.1°$ increments using $\Delta\theta = \pm 0.1°$ windows (giving a 50% spatial overlap). Note that because the windows are defined by $\Delta\theta$ and the traverse speed is constant, the actual time used in the Fourier transform varies with angle from approximately 0.08 seconds at broadside angles to 0.3 seconds at the far inlet and exhaust angles. Figure 4(a) shows the directivity at the blade passing tone[5]. The continuous scan data provides a much richer description of the tone directivity compared to the fixed-stop ($\theta = 2.5°$ increments) data. In contrast, Figure 4(b) shows the same data but at a broadband frequency (i.e. no tones). In this case, there is little directivity in the broadband noise to resolve and the short time records result in a significant increase in the scatter as the statistics are not converged (a slower scan speed or a more advanced processing method could reduce the scatter in the continuous scan results).

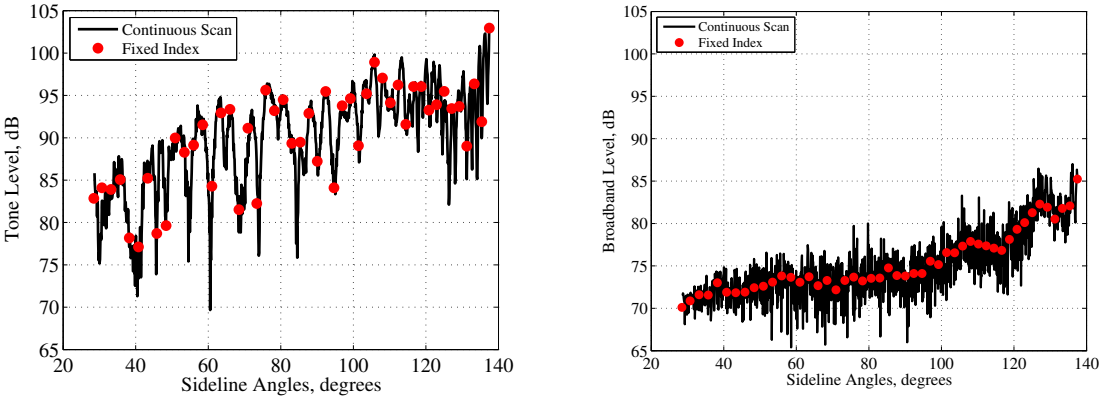

(a) Blade-passing tone (3760 Hz).

(b) Broadband (3600 Hz).

Figure 4: Example directivity measured using fixed index and continuous scan microphone methods.

2.5 Microphone Windscreens

The 9x15 LSWT is a closed-wall wind tunnel and, therefore, noise measurements are make using in-flow microphones equipped with windscreens (also called a "nose" cone by Mueller[16] or an "aerodynamic microphone forebody" (AMF) by Allen and Soderman[18]). Windscreens (Figure 5) reduce the unsteady aerodynamic pressure on the microphone diaphragm while allowing acoustics pressures to excite the diaphragm. A windscreen generally consists of a forebody, shaped to smooth the flow around the microphone, and wire mesh grid near the microphone that allow acoustic waves to enter a small cavity above the diaphragm (Figure 6). The spectral characteristics of a windscreen design depend on the shape of the forebody, speed of the surrounding flow, relative angle to the sound source, and geometry of the internal cavity. Figure 7 shows spectra measured at different flow speeds using three different windscreens.

[3]The 1-inch/second speed provides the best balance between data quality and reduced run time in the experiments conducted to date.

[4]These data points were acquired using the same fan model and test conditions on the same day approximately 15 minutes apart.

[5]Specifically, this is the sum of the narrowband frequency bins containing the blade passing frequency.

The tunnel flow in a fan model test is used to ensure that the flow entering the fan is representative of the flow an aircraft encounters at takeoff or approach. Thus, fan model testing in the 9x15 LSWT has historically used Mach 0.1 as the standard tunnel speed. The Brüel and Kjær UA-0385 windscreen was designed for use in low-speed flows and, therefore, works well in a Mach 0.1 tunnel (Figure 7(a)). However, a recent series of test entries required a Mach 0.2 tunnel speed; at Mach 0.2 the flow instabilities over the UA-0385 windscreen produce high-amplitude spectral effects at frequencies above 20 kHz (Figure 7(d)). Frequency scales linearly with model-scale factor and, therefore, models in the 9x15 LSWT often require data up to 50 kHz in order to project the model-scale results to a full-scale prediction.

Two independent research programs in the 1990's, one at the NASA Ames Research Center (ARC)[18][19] and one at Netherlands Aerospace Centre (NLR)[20], studied windscreen design in an effort to reduce spectral effects related to flow instabilities over the windscreen forebody; each produced a new geometry to mitigate the aerodynamic self-excitation that causes the objectionable signal. The Flow-Induced Tone Eliminator (FITE) windscreen, designed at NASA ARC, features a longer forward section with a more gradual transition upstream of the screen section to reduce the fluctuating pressure over the screen section. The FITE microphone forebodies were created by milling down and threading the forward section of a Brüel and Kjær 6.35 mm (1/4 inch) UA-0385 windscreen so that the new forward section could be attached without changing the screen or internal cavity where the microphone diaphragm resides [18]. The NLR design was commercialized by microphone company G.R.A.S., with part number RA0022 suitable for 6.35 mm (1/4 inch) microphones. The three AMFs are shown in Figure 6.

Representative Brüel and Kjær UA-0385, FITE, and G.R.A.S. RA0022 windscreens were compared during an empty (no model) background noise test in the 9x15 LSWT (2011). Data were acquired at four tunnel Mach numbers ($M = 0.10, 0.15, 0.18, 0.20$). The results (Figure 7) show differences as tunnel Mach number increases in three frequency (f) ranges: $f < 1$ kHz, 1 kHz $\leq f \leq 18$ kHz, and $f > 18$ kHz. In the first frequency range ($f < 1$ kHz), the differences, most prominent at $M = 0.1$, are are now believed to be caused by changes to the tunnel flow-control doors upstream of the test section and not due to the differences between the windscreeens themselves[6]. The measured spectra is independent of windscreen in the second frequency range (1 kHz $\leq f \leq 18$ kHz) at all tunnel Mach numbers. These two frequency ranges, combined ($f \leq 18$ kHz) cover most of the audible spectrum; any of the three windscreens could be used if only audible frequencies are of interest. However, significant spectral differences appear in the third frequency range ($f >$ 18 kHz) as the tunnel Mach number increases.

The Brüel and Kjær UA-0385 windscreen offers a good example of the flow instability problem at high frequencies ($f > 20$ kHz). At $M = 0.15$ (Figure 7(b)), flow instabilities over the wire mesh in front of the microphone appear in the measured spectra as a 20 dB amplification over approximately 1.8 kHz centered at 20 kHz. This spectral feature increases in frequency as the tunnel Mach number increases (Figures 7(c)-7(d)) but is similar in amplitude and spectral width. The Brüel and Kjær UA-0385 forebody was designed for low-speed flows; the FITE windscreen, which has forebody shape designed for higher-speed flows but is otherwise the same, shows no trace of these flow instability effects. The G.R.A.S. RA0022 windscreen is a significant improvement over the Brüel and Kjær windscreen at the higher Mach numbers but a small non-linear response is still produced in the 15 kHz $\leq f \leq 25$ kHz range.

All microphone windscreens are sensitive to manufacturing tolerances[18, 19, 20], especially at high frequencies ($f > 20$ kHz), and require care in handling and installation[7]. Both G.R.A.S. and Brüel and Kjær provide corrections as a function of frequency and incidence angle to the sound source for their windscreens (applicable up to a design Mach number). The FITE windscreens were designed and manufactured as part of a research project and, therefore, manufacturer's calibrations were not available. The FITE windscreens, therefore, were calibrated at the NASA GRC using the method described in Section 2.6).

2.6 Windscreen Calibration

In the same way that each microphone has a unique frequency response that depends on its design, manufacturing tolerances and usage history, each aerodynamic microphone forebody (AMF) has unique frequency

[6]This test was run in conjunction with a test in the 8x6 SWT; the door settings were dictated by the flow requirements in the 8x6 SWT test section.

[7]A few of the new FITE windscreens built after this test were found to exhibit minor flow instability effects; these have been excluded from use in the 9x15 LSWT.

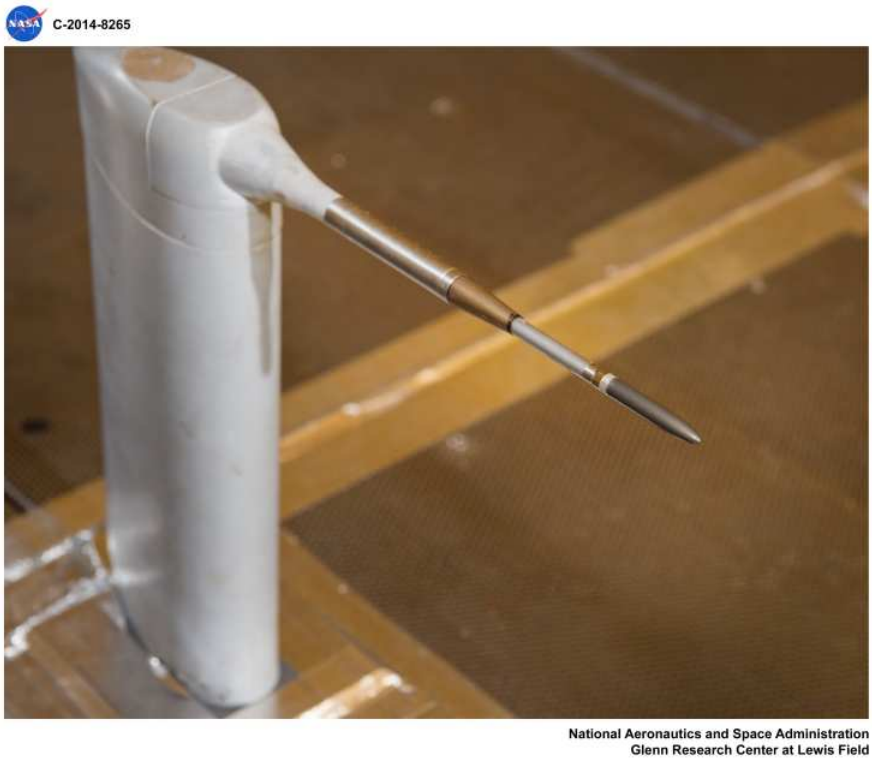

Figure 5: A FITE windscreen on a Brüel and Kjær 4939 6.35 mm (1/4 inch) microphone with a Falcon Range Type 2670 6.35 mm (1/4 inch) pre-amplifier supported by a short stand in the 9x15 LSWT. NASA Image C-2014-8265.

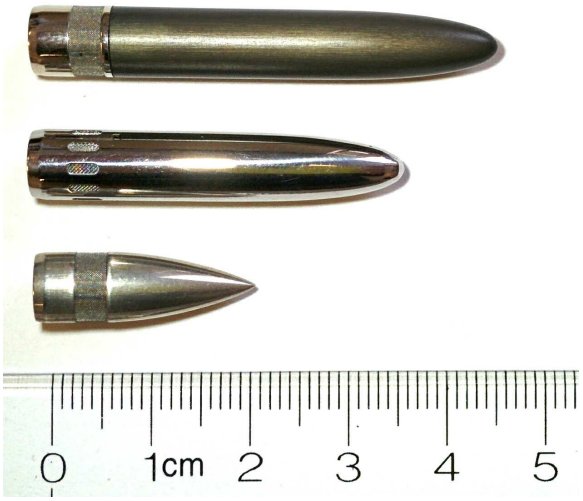

Figure 6: Three aerodynamic microphone forebodies. Top to bottom: FITE, GRAS, Brüel and Kjær.

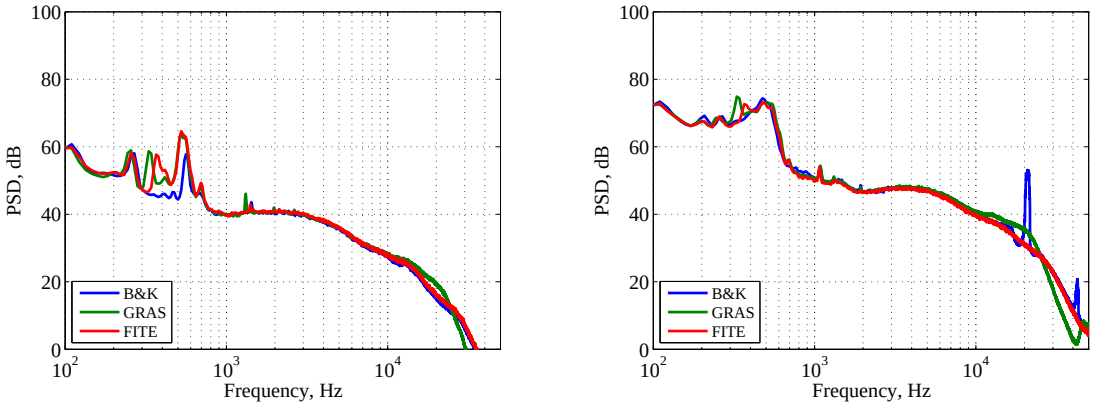

(a) Mach 0.10.

(b) Mach 0.15.

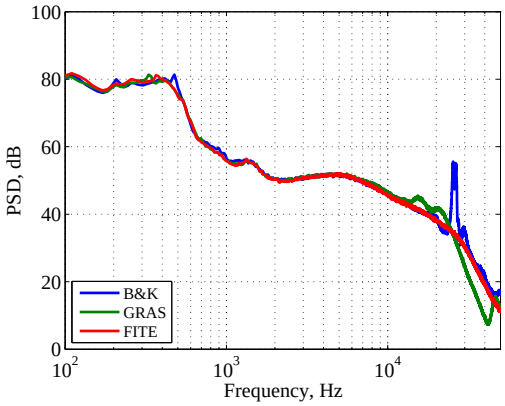

(c) Mach 0.18.

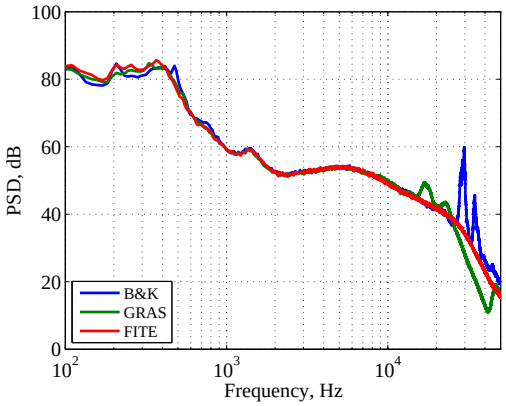

(d) Mach 0.20.

Figure 7: Measured pressure spectra for different windscreens.

response characteristics that depend on these same factors. These characteristics combine to bias an acoustics measurement if they are not accounted for by calibration corrections when the data are processed. The method used at GRC for calibrating and correcting the microphone and windscreen combination follows that described by Allen and Soderman[19, 16], although a tweeter was used instead of an air source. Results were found to be similar to those presented by Allen and Soderman[19]. The methods are explained briefly in the present report.

The newly manufactured windscreens were calibrated in the Acoustical Testing Laboratory[21] at NASA GRC. The sound source was a HiVi RT2H-A Planar Isodynamic Tweeter driven by a Yamaha P1600 power amplifier. This combination was chosen for producing a relatively flat pressure spectra (less than 10 dB down) out to 40 kHz. A Stanford Research Systems DS360 function generator was used to provide a white noise signal. An audio-grade 40μF capacitor was used to provide a high-pass filter. The microphone diaphragm was positioned over the axis of rotation of the turntable. A Brüel and Kjær UA 1588 microphone holder was used to hold the microphone and windscreen horizontally, with the result that a 1/4" vertical cylinder was approximately 5" behind the microphone when positioned at 0°. The test used a National Instruments 9222 analog input C Series module with a cDAQ-9188 chassis as a data recorder. A Newport PMC400 Motion Controller was used to control the Newport 495 rotary turntable. The microphone on the turntable is shown in Figure 8. The speaker was placed about 1 meter away. A larger spatial separation would have been better because the tweeter was fairly large, but the microphone holder and turntable setup was found to be a source of unwanted reflections, necessitating a closer spacing. A modified setup may be investigated in the future.

Figure 8: Windscreen calibrator setup.

The microphones used in the 9x15 LSWT are typically *free-field* microphones. A free-field microphone is designed so that the spectral response is flat (independent of frequency) when used in open space with no protective cover. However, as mentioned above, manufacturing tolerances, deployment history and other factors mean that the free-field correction, denoted $H_{FR}(f)$, is not perfectly flat. Therefore, the free-field response function is provided by the manufacturer with each individual microphone as a deviation (Δ) from the ideal flat response. When used with a windscreen, the microphone response is dramatically changed. The measured autospectra, G_{AMF}, contains the autospectra of the sound source adjusted by the pressure response of the microphone, $H_{PR(f)}$, and the influence of the microphone forebody, $H_{AMF}(\theta_i, f)$, both functions of frequency. However, the acoustic properties of a given windscreen will also depend on the orientation of the windscreen relative to the incident sound waves. The correction, therefore, must also be a function of

incident angle θ_i. The free-field measurements, which are used as a reference to show the effect of the AMF, are only required at one incident angle for which $\theta_i = 0°$ is chosen. The microphone frequency response term is related to the physical properties of the microphone diaphragm and, thus is only a function of frequency. This relationship can be written mathematically as:

$$G_{AMF}(\theta_i, f) = G_{FR}(f) + H_{AMF}(\theta_i, f), \tag{1}$$

where all units are in decibels.

The calibration procedure was to first record the sound from the speaker with the bare microphone oriented directly at the speaker, giving $G_{FR}(f)$. Then the windscreen was installed and recordings were made as a function of turntable rotation in 10 degree increments. Each recording was 10 seconds in length and sampled at 200 kHz, although the speaker signal is very weak above about 80 kHz. A reference microphone was used to verify that the speaker output was constant during the calibration procedure, which took about 15 minutes per windscreen. Once acquired, the time series data were transformed to the frequency domain using a standard fast Fourier transform routine with 2^{10} point Kaiser windows to give a spectral resolution of 195.3 Hz. Note that a relatively small window is used to provide frequency smoothing before computing the correction. For each incident angle θ_i, the sound spectra measured with the bare microphone at 0°, $G_{FR}(f)$ was subtracted from the spectra measured with the windscreen, $G_{AMF}(\theta_i, f)$, to give $H_{AMF}(\theta_i, f)$ per Equation 1.

Example measurements and results are given in Figure 9. Figure 9 (a) shows the measured sound from the tweeter, first with the microphone in the "reference" configuration with the bare diaphragm pointed directly at the tweeter, then with the FITE windscreen installed and pointed at 90º to the speaker. This is a typical geometric configuration of interest when making measurements of a model in the wind tunnel, with the microphone at the same streamwise location in the tunnel as the model, but at a different spanwise location. For a fan model in the 9x15 LSWT, this represents an engine flying directly over an observer.

Figure 9 (b) shows the correction at 90° for a windscreen. Sample results for all windscreens are given in the Appendix. These corrections are individually tracked and applied when the acoustic data are processed. The differences in the correction curves are attributed principally to the manufacturing and assembly tolerances of the small parts. The precise uncertainty of the calibration method has not yet been determined. To apply the correction to wind tunnel data measured with a windscreen $G_{AMF}(\theta_i, f)$, the expression to use is

$$G(f) = G_{AMF}(\theta_i, f) - H_{AMF}(\theta_i, f) - H_{FR}(f). \tag{2}$$

This equation adjusts the measured spectra to that which would be acquired using a free-field microphone at $\theta = 0°$ incidence angle.

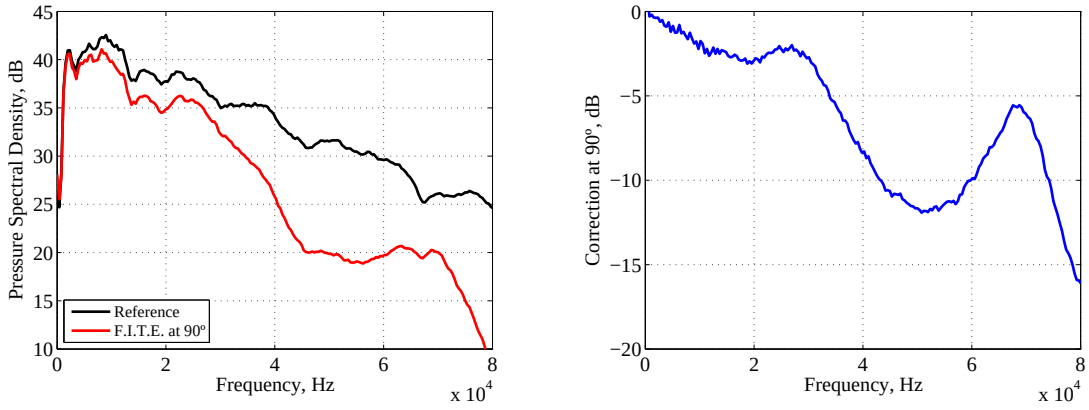

(a) Example Calibration Data

(b) Example Calibration Curve

Figure 9: Spectra acquired with a reference (no AMF) microphone and with a FITE AMF (a) and the resulting AMF correction, H_{AMF} (b).

2.7 Microphone Data Corrections

Data processing is carried out using the Digital Acoustics Data System (DADS) software package developed by the NASA Glenn Acoustics Branch. The DADS software converts the proprietary DataMAX files into individual files for each instrument, and stores them in a simple binary format. The microphone sensitivity determined by a daily pistonphone calibration is also applied, resulting in calibrated time records of pressure in Pascals.

The time records, in Pascals, are transformed to narrowband power spectral density (PSD) functions, typically using 2^{14} point Hanning window[8] functions with 50% overlap, with a 12.2 Hz spectral resolution (at standard 200 kHz sample rate). These are called the "as measured" spectra. The spectra are then corrected for the microphone response, using the manufacturer supplied actuator response curve and the AMF calibration (either supplied by the manufacturer or, for the FITE AMFs, determined using the data in Section 2.6) giving the "instrument corrected" spectra. The angle used for the incident angle to the microphone is computed from the sound emission angle, θ_e, which is a function of the free stream Mach number, M_0 and the geometric angle (θ_g) between the center of the sound source and the microphone,

$$\theta_e = \theta_g - \arcsin\left(M_0 \sin\left(\theta_g\right)\right), \tag{3}$$

assuming linear propagation. The microphone incidence angle is simply $\theta_i = \pi - \theta_e$ using the geometry shown in Figure 10.

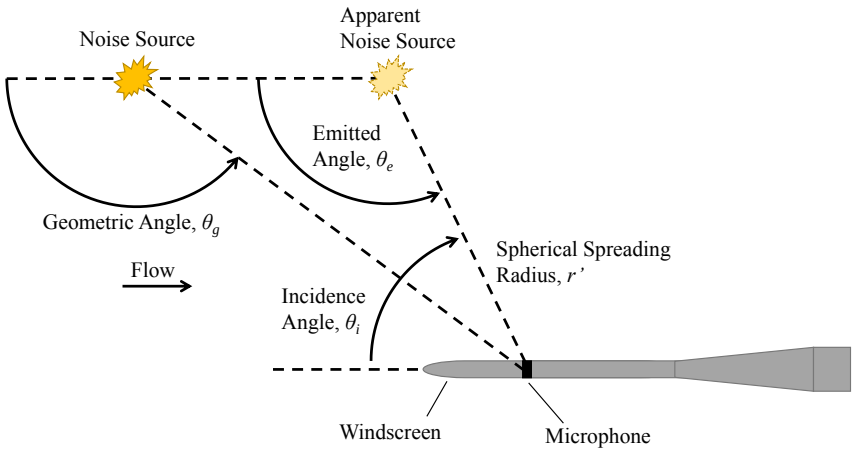

Figure 10: Geometry for inflow microphone measurements.

Subsequently, the spectra are projected onto a 1-foot radius arc and are adjusted to remove losses due to the atmospheric absorption of sound using the recommended ANSI correction[22] and the "as measured" atmospheric conditions (i.e. temperature, humidity, pressure); these results are referred to as "1-foot lossless" spectra. Note that the radius for correction is r', as shown in Figure 10. Ambient temperatures and pressures are recorded by the facility steady-state data system and are provided to the acoustic processing system as a plain text data file. The data at each step (time series, as measured, instrument corrected, 1-ft lossless) is saved for later review, post-processing and analysis. The accuracy of the data system has been assessed as ± 1 dB[23].

[8]Hanning window functions are the default in the 9x15 LSWT data processing routine. Rectangular, Hamming, Blackman, Kaiser, and Flat Top window functions are also available.

3 Data Post-Processing

The standard level of data processing is to 1-foot lossless spectra: from this level, post-processing according to the test requirements can proceed. Post-processing is typically required if the data is to be compared against measurements acquired in a different facility or with a different model. Alternatively, the data might be scaled for size and/or shaft speed to predict a full-scale noise metric. Two examples are given in this section.

3.1 Effective Perceived Noise Level

A common noise metric for commercial aircraft is the Effective Perceived Noise Level (EPNL). This is defined by the Federal Aviation Regulations (FAR) part 36[24]. It describes a method for computing a noise metric from a sound recording made during an aircraft flyover. As part of its decades-long effort in aircraft noise reduction, NASA has developed an Aircraft Noise Prediction Program (ANOPP) to conduct simulated flyovers. The program was first developed in the late 1970's, and has been continuously improved and appended, and has recently been integrated into a larger acoustics package called ANOPP2[25]. ANOPP includes built-in noise models that can be used to predict noise from aircraft engines, and also provides methods allowing noise data from an external source to be used. ANOPP handles geometry calculations and noise propagation between an aircraft flying a given trajectory and an observer on the ground. Atmospheric attenuation, doppler shift, throttle settings and other effects can be accounted for. A description of the steps involved in using acoustic measurements from the 9x15 LSWT to predict aircraft noise using ANOPP is given by Berton[26]. Alternatively, the DADS acoustic data processing software includes programs to project the noise from the 1-foot lossless condition to a different scale-factor, propagate to a flyover distance given a simple set of atmospheric conditions, and compute the EPNL from the results.

3.2 Calculation of Sound Power

The acoustic power can be estimated using the microphone measurements of the radiated sound. Appropriate starting expressions are given on page 41 of Goldstein[27]. The acoustic power is the integral of time-averaged acoustic intensity flux through a closed surface,

$$\Pi = \int_S \bar{\mathbf{I}} \cdot \mathbf{n} dS \tag{4}$$

The expression for acoustic intensity should include the effect of the tunnel mean flow,

$$\mathbf{V_0} = V_0 \mathbf{e}_x \tag{5}$$

which is assumed to be potential. The intensity is then given as

$$\mathbf{I} = \left(\frac{p'}{\rho_0} + \mathbf{u}' \cdot \mathbf{V_0} \right) (\rho_0 \mathbf{u}' + \rho' \mathbf{V_0}) \tag{6}$$

and the follow approximations for acoustic perturbations are assumed to apply,

$$\mathbf{u}' = u' \mathbf{e}_{r_e}, \quad u' = \tfrac{p'}{\rho_0 c_0} \quad \text{and } \rho' = \tfrac{p'}{c_0^2}$$

Substituting,

$$\mathbf{I} = \frac{p'^2}{\rho_0 c_0} \mathbf{e}_{r_e} + \frac{p'^2}{\rho_0 c_0} M_0 \mathbf{e}_x + \frac{p'^2}{\rho_0 c_0} M_0 \left(\mathbf{e}_{r_e} \cdot \mathbf{e}_x \right) \mathbf{e}_{r_e} + \frac{p'^2}{\rho_0 c_0} M_0^2 \left(\mathbf{e}_{r_e} \cdot \mathbf{e}_x \right) \mathbf{e}_x \tag{7}$$

where,

$$\mathbf{e}_x = -\cos\theta_e \mathbf{e}_{r_e} \tag{8}$$

gives,

$$\bar{\mathbf{I}} \cdot \mathbf{n} = \bar{\mathbf{I}} \cdot \mathbf{e}_{r_e} = \frac{\bar{p}'^2}{\rho_0 c_0} \left(1 - 2 M_0 \cos\theta_e + M_0^2 \cos^2\theta_e \right) \mathbf{e}_{\mathbf{r_e}} \cdot \mathbf{e}_{\mathbf{r_e}} = \left(1 - M_0 \cos\theta_e \right)^2 \frac{\bar{p}'^2}{\rho_0 c_0} \tag{9}$$

where $(1 - M_0 \cos\theta_e)^2$ is the tunnel convection effect and θ_e is the radiated noise emission angle defined in Equation 3. These are the two differences caused by the mean convection. Substituting back into Equation 4 and integrating over the surface of a sphere of radius r, this gives,

$$\Pi = \frac{1}{\rho_0 c_0} \int_0^{2\pi} \int_0^{\pi} r^2 \bar{p'}^2 (r, \theta_e) (1 - M_0 \cos\theta_e)^2 \sin(\theta_e) \, d\theta_e d\phi \tag{10}$$

Since measurements are typically only available on a sideline, azimuthal symmetry is assumed giving

$$\Pi = \frac{2\pi}{\rho_0 c_0} \int_0^{\pi} r^2 \bar{p'}^2 (r, \theta_e) (1 - M_0 \cos\theta_e)^2 \sin(\theta_e) \, d\theta_e \tag{11}$$

This expression can be easily evaluated using trapezodial integration and the one-foot lossless data output from the DADS code, as described in Section 2.7. As a practical matter, the speed of sound in the tunnel can be closely approximated in meters per second using the measured static temperature in Rankine,

$$c_0 = 165.6 + 0.337 \, T_s \tag{12}$$

while the air density in kg/m^3 can be similarly calculated using the ambient static pressure in pounds per square inch and ambient temperature in Rankine,

$$\rho_0 = 43.2 \frac{p_s}{T_s} \tag{13}$$

As the sound is only measured between approximately 30° from upstream to 135° from upstream (or 160°, if all three aft microphones are used), the limits of integration in Equation 11 do not extend all the way between 0 and π. The typical microphone layout was discussed in Section 2.1. Sound radiating outside the measured limits is typically neglected, but some extrapolation of the measured directivy could also be used. Also note that the decibel reference power is one picowatt (1^{-12} W).

4 Other Acoustic Instrumentation

A number of other acoustic measurement techniques have been used in the 9x15 LSWT, either for specific tests or as research items. This section describes five additional acoustic instruments that have been used in the last 10 years.

4.1 Linear Array

A linear array of microphones with 16 streamwise measurement locations was built in 2009. The idea was to acquire data simultaneously at all 16 polar angles without wake interference from the upstream microphones. Each measurement location used three flush-mounted microphones mounted vertically as pictured in Figure 11. The top and bottom microphones are each offset 5 cm (2 in) vertically from the center microphone. The flush-mounted microphones will record both sound from the model being tested and unsteady hydrodynamic pressures from the boundary layer flow over the array surface. This design assumes that the noise from the model is coherent over the 10 cm distance between the top and bottom microphones while the boundary layer noise is incoherent over the same distance. Signal processing is then used to reject the boundary layer noise while retaining the noise generated by the model. A rendered graphic showing the installation of the linear array during the open rotor wind tunnel test is given in Figure 12. The array is mounted from the south wall of the wind tunnel using two large arms, designed to hold the face of the array 1.52 meters (5 feet) from the centerline of a drive rig mounted in the usual location.

This instrument allows extremely rapid data acquisition, compared with the moving traverse, as all sensors are sampled simultaneously. The angular directivity is less, and there are challenges using signal processing to reject the boundary layer flow over the sensors.[28] Specifically, broadband noise from a model may be lost under the unsteady aerodynamic pressures in the boundary layer over the array and the maximum frequency measurable by the array is dictated by the vertical spacing between the microphones at each station. A sample result (up to 10 kHz) is shown in Figure 13, where the magnitude of the cross spectrum

Figure 11: Linear array of flush-mounted microphones.

recorded by the linear array microphones at 90° is compared with the single traversing microphone at the same geometric angle. Generally, the tone levels match reasonably well, while the broadband is a good match at some frequencies and a poor match at others.

A small linear array was built as a test article, pictured in Figure 14. This hardware was installed in the wind tunnel to evaluate alternatives to flush-mounting the linear-array microphones. It could be adapted as a research instrument for future linear-array work.

4.2 Phased Array

The phased-array is another instrument that has been used successfully in the 9x15 LSWT (Figure 15). This array can be installed in either side wall of the wind tunnel, perpendicular to the model to be studied. A Kevlar cloth "window" can be used to cover the array, shielding it from the airflow in the tunnel and covering the gap in the tunnel wall. Currently, an Array-48 system from Opivnav is the standard phased-array in the 9x15 LSWT; this array has been used for source localization and has been very effective at identifying sources of unwanted noise. Reports regarding the phased array data acquired in the 9x15 LSWT include[29] and [30]. An example result is given in Figure 16, where it was useful for identifying noise contamination generated by the drive rig turbine at the downstream end of the test section. This result motivated the design and deployment of a drive rig muffler, discussed in a separate report.[31]

4.3 Rotating Rake

NASA has developed a rotating rake system for measuring acoustic modes inside a fan duct [32, 33]. A radial array of unsteady pressure transducers is continuously rotated azimuthally around the fan duct. The radial rake of transducers is supported by a large drum which surrounds the fan model nacelle. The drum is mounted to a set of rails held to the base of the drive rig, as pictured in Figure 17 (a). A single radial rake is typically used, but recent developments include the ability to utilize dual rakes, as shown in Figure 17(b). A rake can be inserted either at the throat of the inlet to measure forward-propagating modes, or at the exit

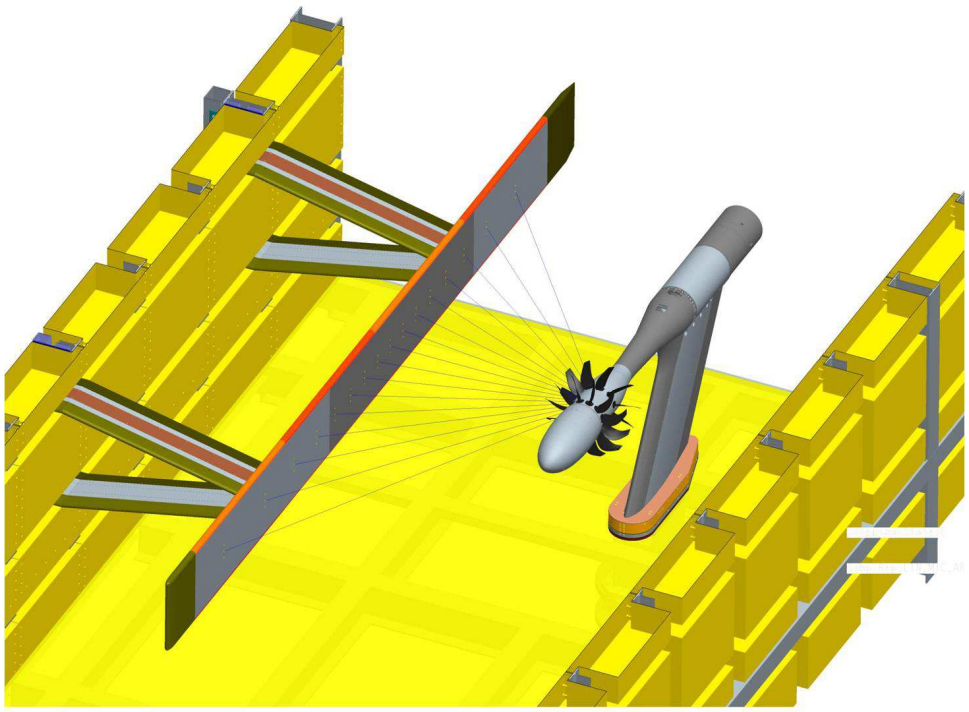

Figure 12: Render of the linear array in the 9x15 LSWT, showing 16 directivity measurement directions from the Open Rotor Propulsion Rig.

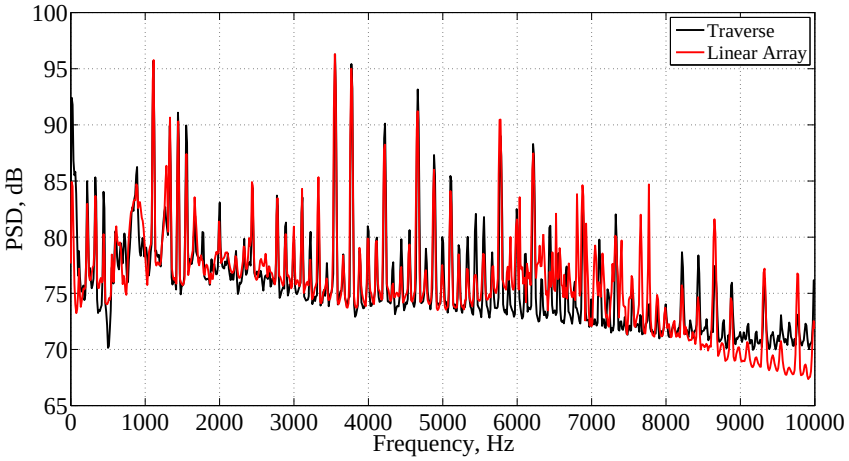

Figure 13: Example result comparing open rotor acoustic measurements acquired with the linear array and traversing microphone.

plane of the bypass nozzle to measure aft-propagating modes. A technique for analyzing data acquired over passive treatment has also been recently developed.[34]

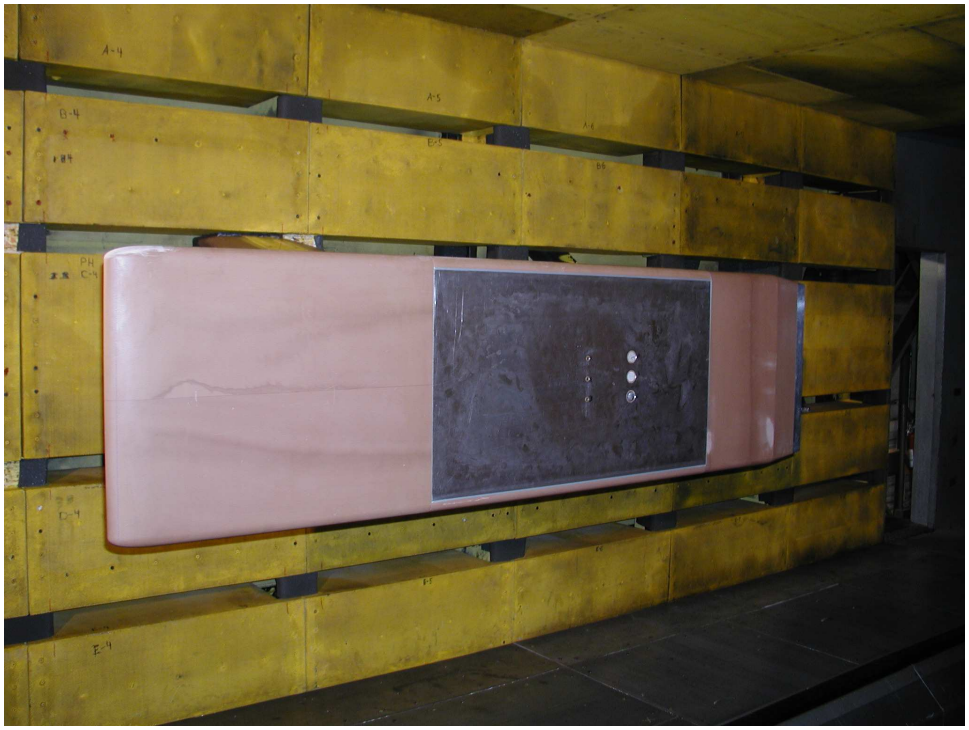

Figure 14: Linear array test article installed in the 9x15 LSWT.

4.4 Internal Unsteady Pressure Measurements

Unsteady pressure transducers are often installed inside a fan model in the 9x15 LSWT, either on rakes that extend into the flow passages, on the fan blades and/or vanes, or embedded in the duct walls. Wireless[35] and wired sensors have both been employed.

4.5 Acoustic Barrier Wall

While not strictly an instrument, a barrier wall is frequently used in the 9x15 LSWT to help isolate noise sources. The wall spans the full height of the tunnel, but can vary in length and streamwise location. A photograph of a barrier wall installed near a fan model is given as Figure 18. In this case, the wall was used to shield the sideline traversing microphone from noise radiated from the aft portion of a fan nacelle. With the wall in place, the microphone is assumed to measure only the inlet radiated noise. The aft radiated noise can thus be inferred, and in the case of tone noise some interference might be observed. A sample result acquired from the Honeywell fan test in 2014 is shown in Figure 19. Another application of the barrier was the 2010 open rotor test when a short barrier wall was used to represent an aircraft surface for shielding experiments.[36, 26]

5 Background Noise Levels

As part of normal acoustic testing procedures, background noise levels in the test section are periodically recorded. Measurements taken many years apart have been found to be very similar, suggesting the background noise measurements are largely stationary in time. Background noise spectra are plotted in Figure 20 and tabulated in Table 2. The noise was found to be largely uniform throughout the wind tunnel test section. The microphone probes are typically mounted between four and seven feet from the model being tested. Prospective users of the tunnel should compare their estimated noise level at these distances to the provided background noise levels.

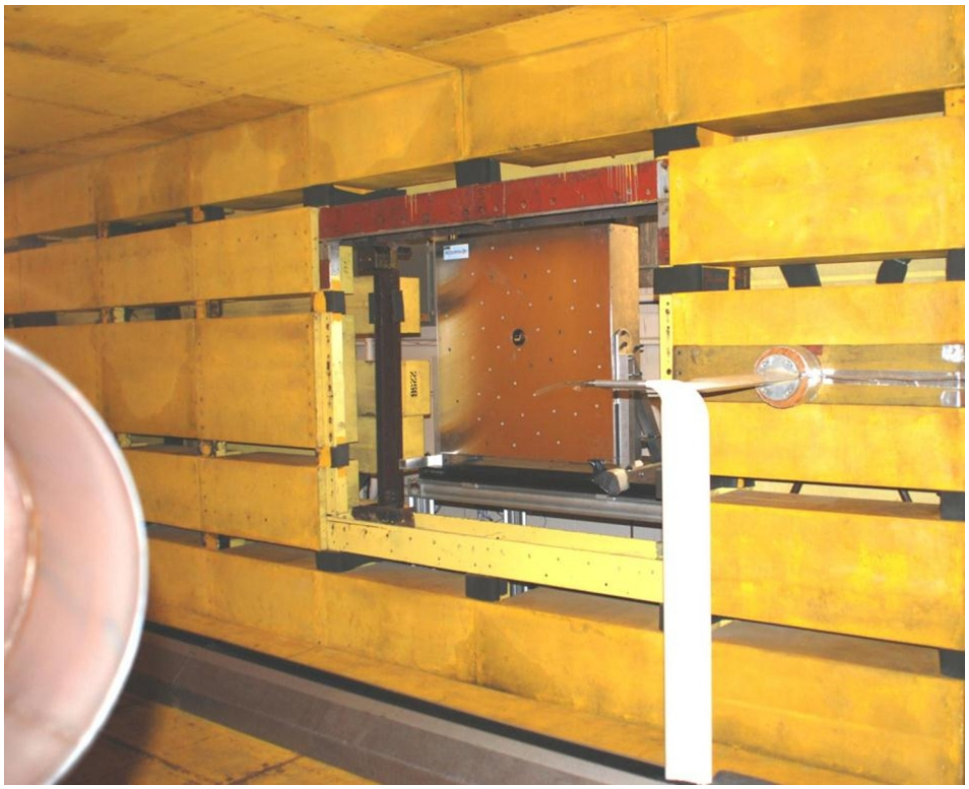

Figure 15: Optinav Array-48 installed in the 9x15 LSWT.

An extensive set of background noise measurements were acquired in February and March 2012 using microphones located throughout the tunnel circuit. During this test, the tunnel was empty except for microphone probes and the requisite pressure and temperature rakes. These data were acquired to support an acoustic assessment of the tunnel by Jacobs Engineering Group, Inc. It also served to document the background noise levels in the tunnel loop at that time. A detailed assessment of this data set is given in Reference [9]. As of November 2016, the 9x15 LSWT is scheduled for a substantial renovation intended to reduce the background noise level. Thus, the background noise spectra presented in this section is only applicable to historical data and a new set of data will be acquired when the modifications are complete (scheduled for 2018).

6 Summary

This report discussed the methods used for acquiring and processing acoustic data in the 9x15 LSWT at NASA GRC. Calibration methods and data correction procedures were described. Other acoustic instruments were briefly discussed and background noise levels in the test section were presented. This report is intended to document the capabilities of the tunnel and its data systems and as a guide for prospective users of the facility.

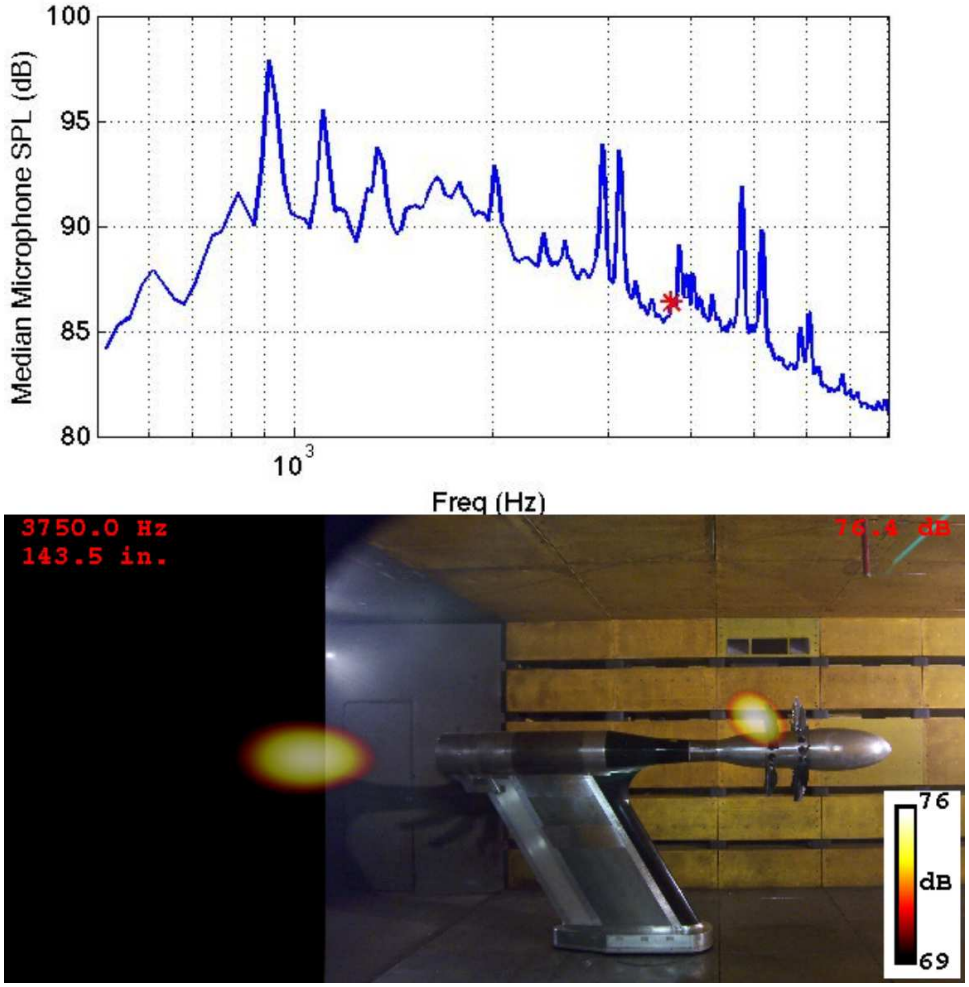

Figure 16: Example result from measuring the open rotor with the phased array.

(a) Rotating rake installed over a fan model in the 9x15 LSWT.

(b) Close view of dual rotating microphone rakes.

Figure 17: Pictures of the rotating rake system used for fan models in the 9x15 LSWT.

Figure 18: Barrier wall installed in the 9x15 LSWT.

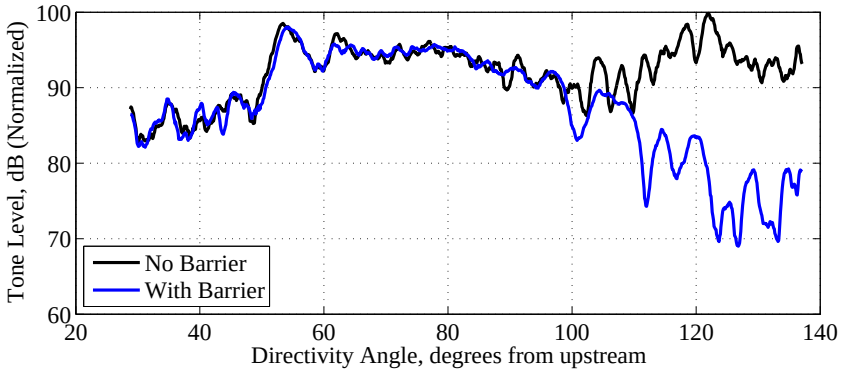

Figure 19: Continuous scan measurement of a fan tone with and without the acoustic barrier wall in place.

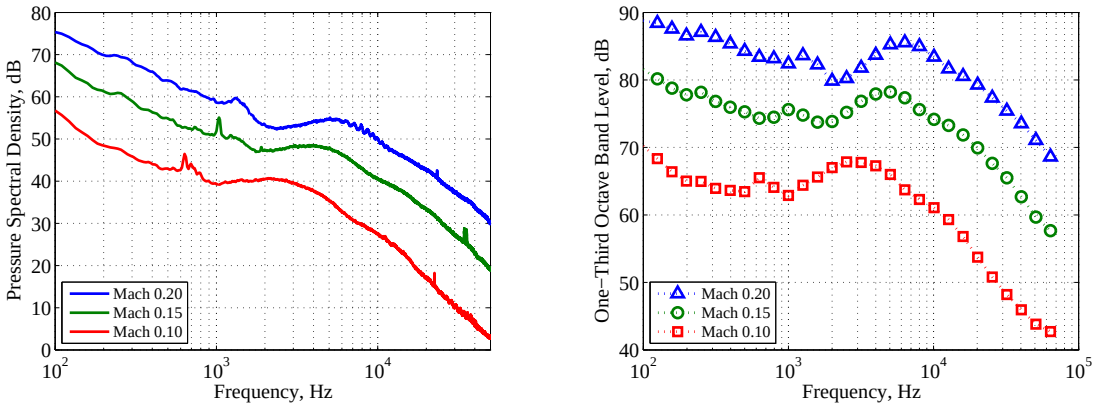

(a) Narrowband

(b) One-Third Octave Band

Figure 20: 9x15 Background Noise Levels.

Table 2: One-Third Octave Band Data from Figure 20.

Freq, Hz	Mach 0.10	Mach 0.15	Mach 0.20
39	81.5	91.5	98.7
50	79.5	88.7	95.3
62	75.5	84.6	91.6
79	71.1	81.4	88.4
99	70.3	81.6	88.8
125	68.3	80.2	88.4
157	66.4	78.8	87.6
198	65.0	77.8	86.5
250	65.0	78.2	87.1
315	63.9	76.8	86.3
397	63.6	76.0	85.4
500	63.5	75.3	84.3
630	65.5	74.3	83.4
794	64.1	74.5	83.2
1000	62.9	75.6	82.4
1260	64.4	74.8	83.6
1587	65.6	73.7	82.3
2000	67.0	73.8	79.9
2520	67.9	75.2	80.2
3175	67.8	76.8	81.8
4000	67.3	77.9	83.7
5040	66.0	78.2	85.2
6350	63.7	77.4	85.5
8000	62.3	75.6	85.0
10079	61.6	74.2	83.4
12699	59.3	73.3	81.7
16000	56.8	71.8	80.6
20159	53.7	69.9	79.3
25398	50.8	67.6	77.3
32000	48.2	65.5	75.4
40317	46.0	62.7	73.5
50797	43.8	59.7	71.1
64000	42.7	57.7	68.6

Acknowledgments

This report was funded by the NASA Advanced Air Transport Technology Project. Dr. Edmane Envia in the GRC Acoustics Branch derived the sound power calculation described in Section 3.2. Gary Podboy and Dave Elliott, also from the GRC Acoustics Branch, served as technical reviewers for this work.

References

[1] Yuska, J. A., Diedrich, J. H., and Clough, N., "Lewis 9- by 15-Foot V/STOL Wind Tunnel," *NASA/TM-X-2305*, July 1971.

[2] Beranek, L. L., Labate, S., and Ingard, U., "Acoustical Treatment of the NACA 8- by 6-Foot Supersonic Propulsion Wind Tunnel," *NACA TN-3378*, June 1955.

[3] Soeder, R. H., "NASA Lewis 9- by 15-foot Low-Speed Wind Tunnel User Manual," *NASA TM-106247*, 1993.

[4] Rentz, P. E., "Softwall acoustical characteristics and measurement capabilities of the NASA Lewis 9x15 foot low speed wind tunnel," *NASA CR-135026*, 1976.

[5] Arrington, A. E. and Gonsalez, J. C., "Calibration of the NASA Lewis Research Center 9- by 15-Foot Low Speed Wind Tunnel (1994 Test)," *NASA CR-195438*, 1997.

[6] Dahl, M. D. and Woodward, R. P., "Comparison between design and installed acoustic characteristics of NASA Lewis 9- by 15-foot low-speed wind tunnel acoustic treatment," *NASA TP-2966*, 1990.

[7] Dahl, M. D. and Woodward, R. P., "Acoustical Evaluation of the NASA Lewis 9- by 15-Foot Low Speed Wind Tunnel," *NASA TP-3274*, 1992.

[8] Woodward, R. P., Dittmar, J. H., Hall, D. G., and Kee-Bowling, B., "Background Noise Levels Measured in the NASA Glenn 9- by 15-Foot Low-Speed Wind Tunnel," *AIAA-95-0720 / NASA TM-106817*, 1995.

[9] Stephens, D. B., "The Acoustic Environment of the NASA Glenn 9- by 15-foot Low-Speed Wind Tunnel. AIAA-2015-2684," *21st AIAA/CEAS Aeroacoustics Conference, Dallas, Texas, USA*, 22-26 June 2015.

[10] Woodward, R. P., Loeffler, I. J., and Dittmar, J. H., "Measured Far-Field Flight Noise of a Counterrotation Turboprop at Cruise Conditions," *NASA/TM-101383*, January 1989.

[11] Stephens, D. B. and Envia, E., "Acoustic Shielding for a Model Scale Counter-rotation Open Rotor. AIAA-2011-2940," *17th AIAA/CEAS Aeroacoustics Conference,, Portland, Oregon, USA*, 5-8 June 2011.

[12] Woodward, R. P., Hughes, C. E., Jeracki, R. J., and Miller, C. J., "Fan Noise Source Diagnostic Test – Far-field Acoustic Results," *AIAA 2002-2427*, 2002.

[13] Balan, C. and Hoff, G. E., "Propulsion Simulator for High Bypass Turbofan Performance Evaluation," *1993 SAE Aerospace Atlantic Conference & Exposition, Dayton Ohio*, April 20-23, 1993.

[14] Delaney, B., Balan, C., West, H., Humenik, F. M., and Crain, G., "A Model Propulsion Simulator for Evaluating Counterrotating Blade Characteristics (SAE 861715)," *Aerospace Technology Conference and Exposition, Long Beach, California, USA*, October 13-16, 1986.

[15] Duell, E., Walter, J., Arnette, S., and Yen, J., "Recent Advances in Large-Scale Aeroacoustic Wind Tunnels," *AIAA 2002-2503*, 2002.

[16] Mueller, T. J., editor, *Aeroacoustic Measurements*, Springer, 2002.

[17] Shah, P. N., Vold, H., Hensley, D., Envia, E., and Stephens, D., "A High-Resolution, Continuous-Scan Acoustic Measurement Method For Turbofan Engine Applications," *J. Turbomach.*, Vol. 137, No. 12, 2014.

[18] Allen, C. S. and Soderman, P. T., "Aeroacoustic Probe Design for Microphone to Reduce Flow-Induced Self-Noise, AIAA 93-4343," *15nd AIAA Aeroacoustics Conference, Long Beach, California, USA*, 25-27 October 1993.

[19] Allen, C. S. and Soderman, P. T., "Microphone Corrections for Accurate In-Flow Acoustic Measurements at High Frequency, CEAS/AIAA 95-150," *1st Joint CEAS/AIAA Aeroacoustics Conference,, Munich, Germany*, 12-15 June 1995.

[20] Dassen, T., Holthusen, H., and Beukema, M., "Design and Testing of a Low Self-Noise Aerodynamic Microphone Forebody," *National Aerospace Laboratory NLR TP 96320*, May 1996.

[21] Cooper, B. A., "Design and construction of a convertible hemi/anechoic acoustical laboratory for testing space flight hardware at the NASA Glenn Research Center," *The Journal of the Acoustical Society of America*, Vol. 108, No. 5, 2000, pp. 2473–2473.

[22] *Method for Calculation of the Absorption of Sound by the Atmosphere, ANSI Standard S1-26:1995*, 1995.

[23] Dahl, M. D., "Assessment of NASA's Aircraft Noise Prediction Capability," *NASA/TP-2012-215653*, 2012.

[24] "Noise standards: Aircraft Type and Airworthiness Certification," *U.S. Code of Federal Regulations, Title 14, Chapter I, Part 36*.

[25] Lopes, L. V. and Burley, C. L., "Design of the Next Generation Aircraft Noise Prediction Program: ANOPP2 AIAA-2011-2854," *NASA NF1676L-11643*, June 2011.

[26] Berton, J. J., "Empennage Noise Shielding Benefits for an Open Rotor Transport AIAA-2011-2764," *17th AIAA/CEAS Aeroacoustics Conference, Portland, Oregon*, 5-8 June 2011.

[27] Goldstein, M. E., *Aeroacoustics*, McGraw-Hill, New York, 1976.

[28] Nance, D. and Ahuja, K., "Limitations of the Three-Microphone Signal Enhancement Technique, AIAA-2007-441," *45th AIAA Aerospace Sciences Meeting and Exhibit, Reno, Nevada*, 8-11 January 2007.

[29] Horváth, C., "Beamforming Investigation of Dominant Counter-Rotating Open Rotor Tonal and Broadband Noise Sources," *AIAA Journal*, Vol. 53, 2015, pp. 1602–1611.

[30] Horváth, C., Envia, E., and Podboy, G. G., "Limitations of Phased Array Beamforming in Open Rotor Noise Source Imaging," *AIAA Journal*, Vol. 52, 2014, pp. 1810–1817.

[31] Stephens, D. B., "Acoustic Performance of Drive Rig Mufflers for Model Scale Engine Testing," *NASA TM-2013-217885*, June 2013.

[32] Sutliff, D. L., "Rotating Rake Mode Measurement System," *NASA TM-2005-213828*, October 2005.

[33] Sutliff, D. L., "Turbofan Duct Mode Measurements Using a Continuously Rotating Microphone Rake," *International Journal of Aeroacoustics*, Vol. 6, 2007, pp. 147–170.

[34] Sutliff, D. L. and Dahl, M. D., "Techniques for analyzing rotating rake mode measurements over passive treatment," *International Journal of Aeroacoustics*, Vol. 15(4-5), 2016, pp. 430–461.

[35] Zaman, A., Bauch, M., and Raible, D., "Embedded Acoustic Sensor Array for Engine Fan Noise Source Diagnostic Test: Feasibility of Noise Telemetry Via Wireless Smart Sensors," *NASA TM-2011-217017*, July 2011.

[36] Stephens, D. B. and Envia, E., "Acoustic Shielding for a Model Scale Counter-rotation Open Rotor," *NASA TM-2012-217227*, January 2012.

Appendix: FITE AMF Corrections as of March 2014

A total of 18 FITE AMFs have been made and a sample of calibration curves for each are shown in this appendix.

An accurate and precise calibration of any measurement device is often difficult to obtain. This is particularly true when a validated test setup is not available as there are many potential sources of uncertainty that may affect the result. The 6.35 mm (1/4 inch) FITE microphone forebodies were calibrated in three separate tests using two facilities and two different sound sources. The test setup and methodology was refined with each entry with the end goal of producing a repeatable frequency calibration. The first test entry, in the Acoustic Test Laboratory (ATL) at the NASA GRC, used a speaker source and a single microphone on a rotating stand. An analysis of these data showed several issues, including sound reflection off the support stand and microphone type used, which were corrected for a second test. Due to facility availability, the second test was conducted in the NASA GRC Aero-Acoustic Propulsion Laboratory (AAPL). This test used a pressurized air noise source and a microphone stand modified to reduce sound reflections which provided more consistent results. Finally, a third test, this one back in the ATL and using the modified microphone stand from the AAPL test, was performed to calibrate a new batch of FITE forebodies. These results were generally consistent with those from the second test. It should be noted that although the forebody correction is theoretically the same for all forebodies with the same shape (one calibration is often provided for an entire class of AMF), small differences were measured between the FITE forebodies and, therefore, calibration curves were determined for each one; the FITE AMFs were manufactured in small numbers so there may be more variation between each one than might be found if they were built in larger numbers using dedicated machines. The results presented here are from the third test entry, since it is the most complete and considered to be the most reliable.

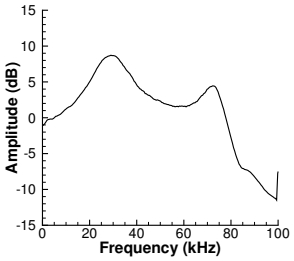

(a) 0°

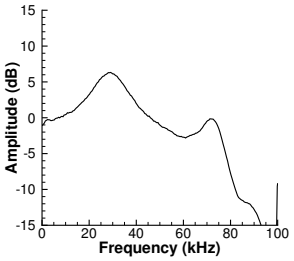

(b) 30°

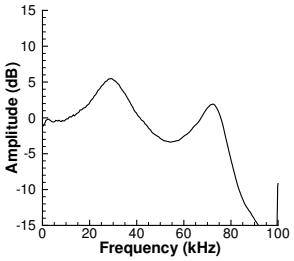

(c) 60°

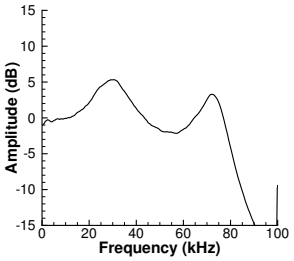

(d) 90°

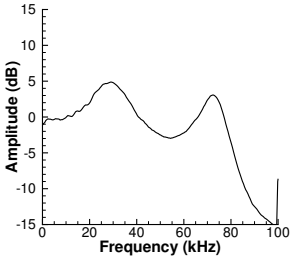

(e) 120°

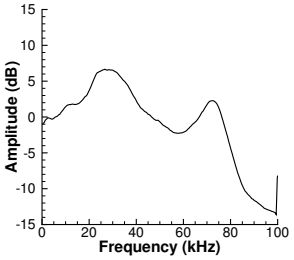

(f) 150°

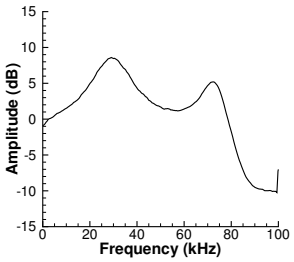

(g) 180°

Figure 21: Correction as of March 2014 for the FITE0001 AMF.

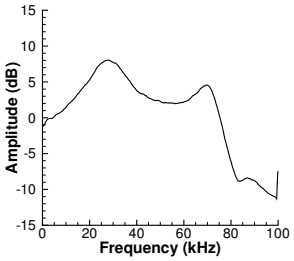

(a) 0°

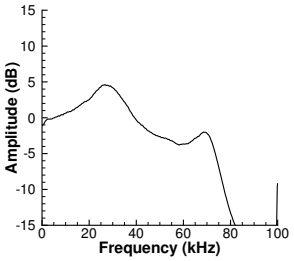

(b) 30°

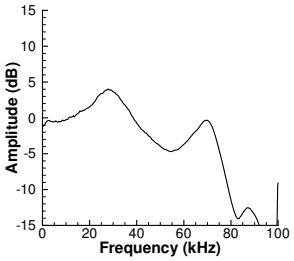

(c) 60°

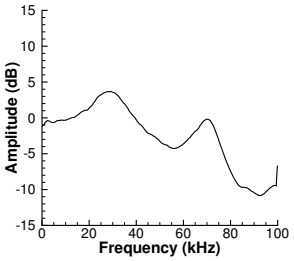

(d) 90°

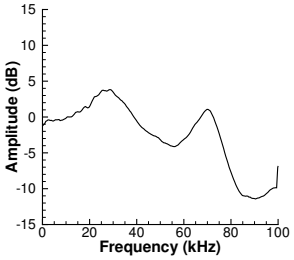

(e) 120°

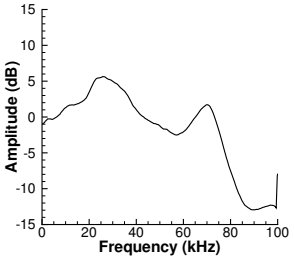

(f) 150°

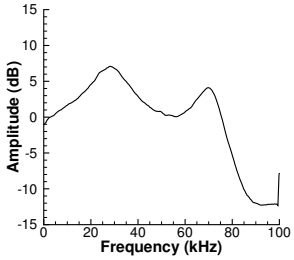

(g) 180°

Figure 22: Correction as of March 2014 for the FITE0002 AMF.

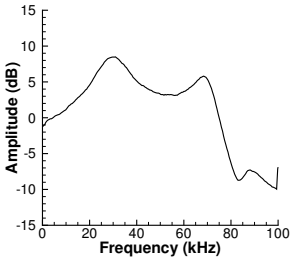

(a) 0°

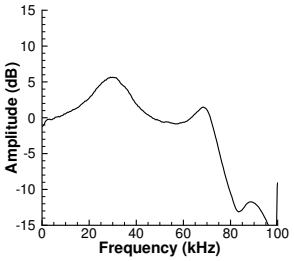

(b) 30°

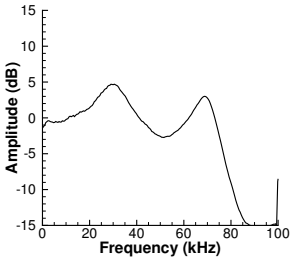

(c) 60°

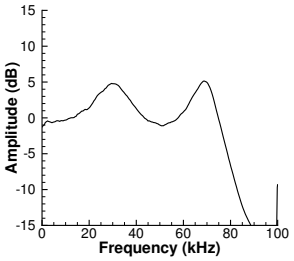

(d) 90°

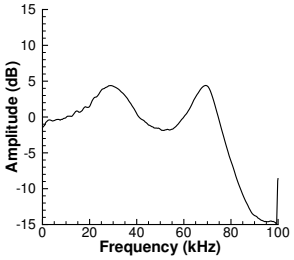

(e) 120°

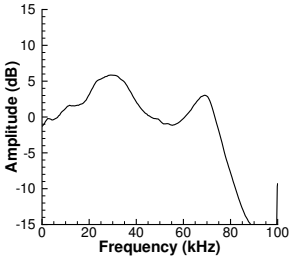

(f) 150°

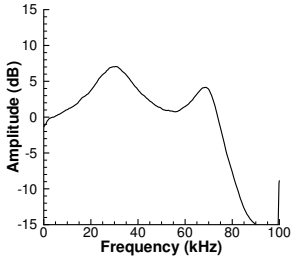

(g) 180°

Figure 23: Correction as of March 2014 for the FITE0003 AMF.

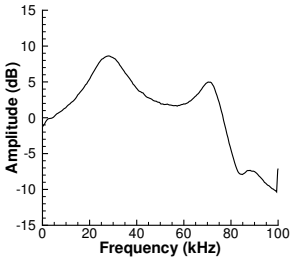

(a) 0°

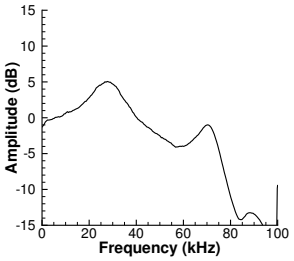

(b) 30°

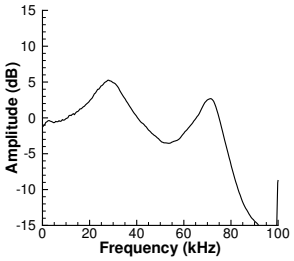

(c) 60°

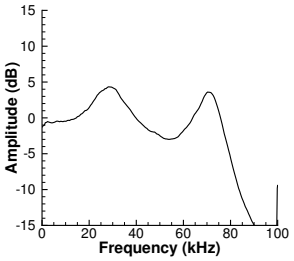

(d) 90°

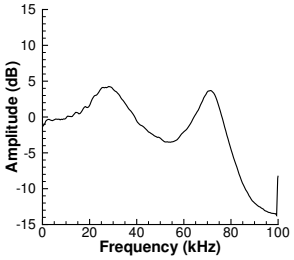

(e) 120°

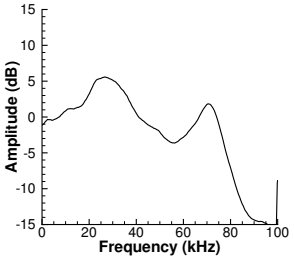

(f) 150°

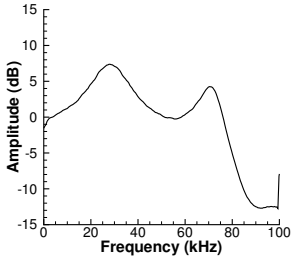

(g) 180°

Figure 24: Correction as of March 2014 for the FITE0004 AMF.

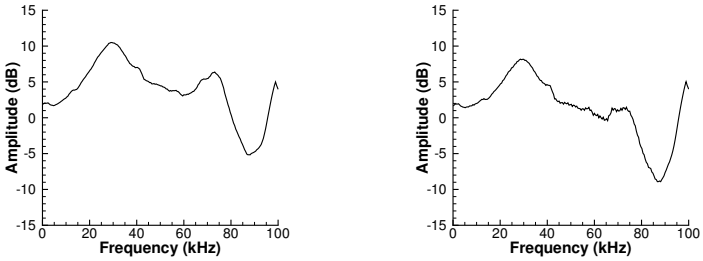

(a) 0°

(b) 30°

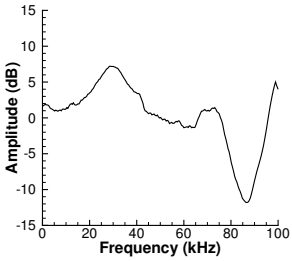

(c) 60°

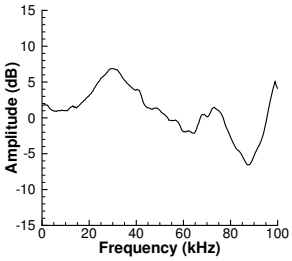

(d) 90°

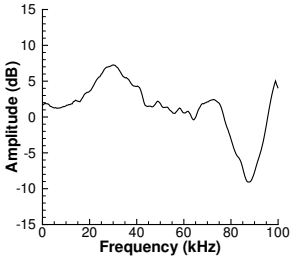

(e) 120°

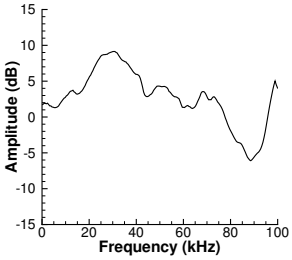

(f) 150°

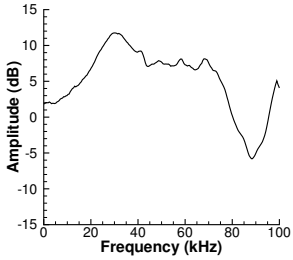

(g) 180°

Figure 25: Correction as of March 2014 for the FITE0005 AMF.

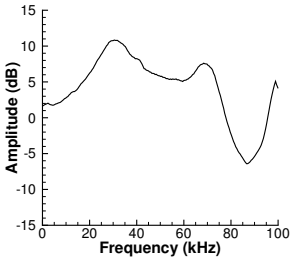

(a) 0°

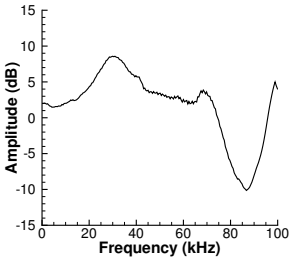

(b) 30°

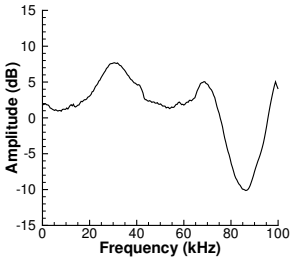

(c) 60°

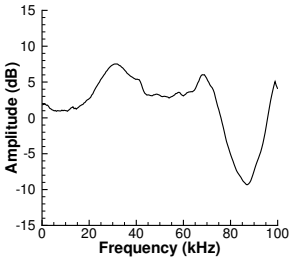

(d) 90°

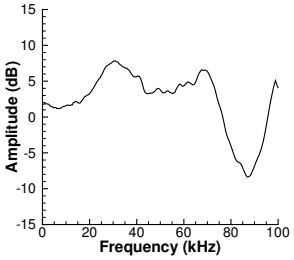

(e) 120°

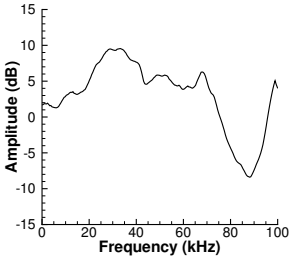

(f) 150°

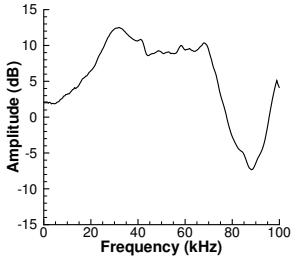

(g) 180°

Figure 26: Correction as of March 2014 for the FITE0006 AMF.

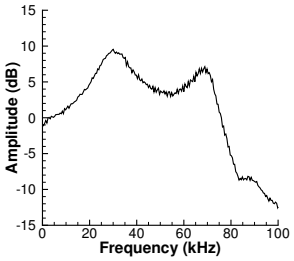

(a) 0°

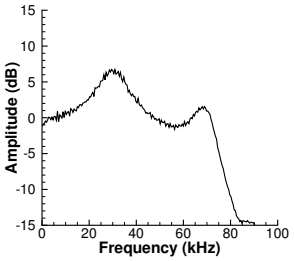

(b) 30°

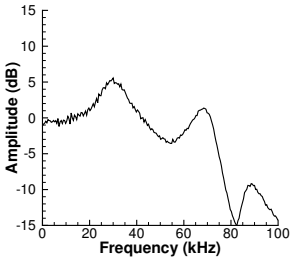

(c) 60°

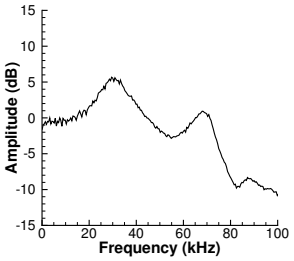

(d) 90°

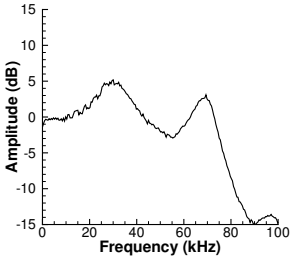

(e) 120°

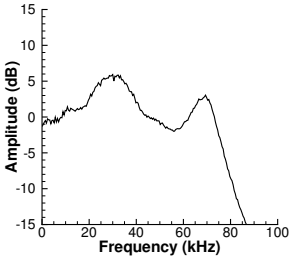

(f) 150°

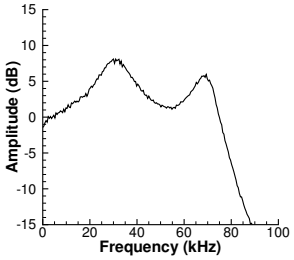

(g) 180°

Figure 27: Correction as of March 2014 for the FITE0007 AMF.

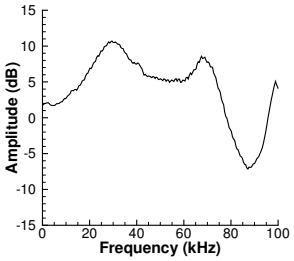

(a) 0°

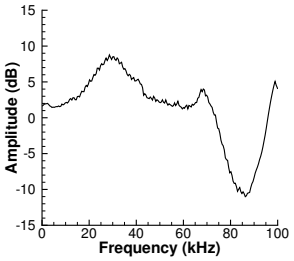

(b) 30°

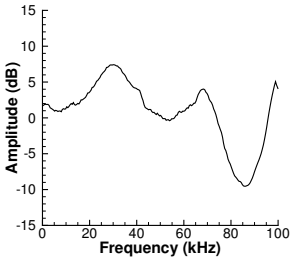

(c) 60°

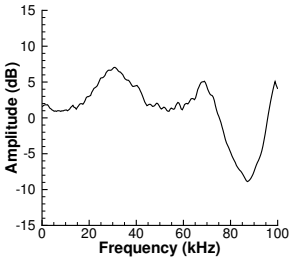

(d) 90°

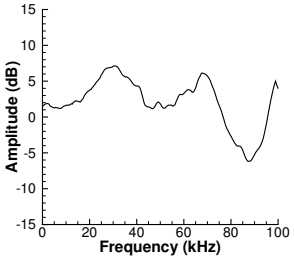

(e) 120°

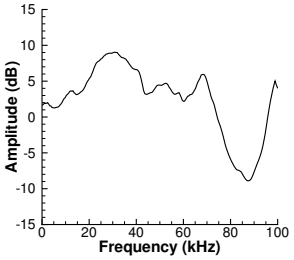

(f) 150°

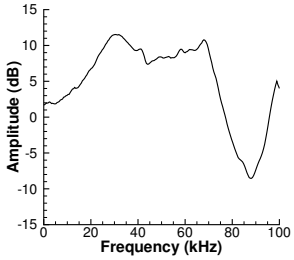

(g) 180°

Figure 28: Correction as of March 2014 for the FITE0008 AMF.

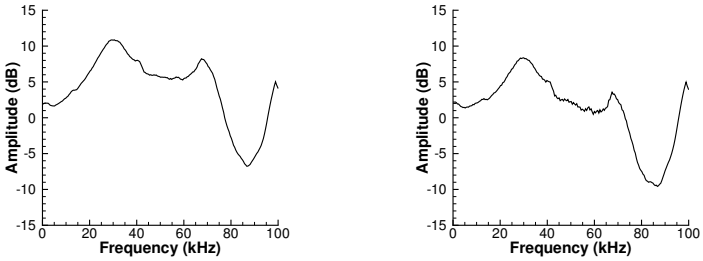

(a) 0°

(b) 30°

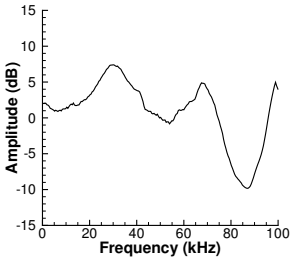

(c) 60°

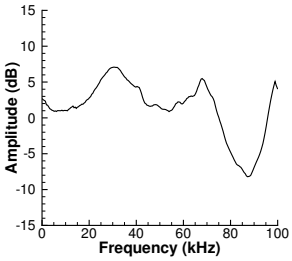

(d) 90°

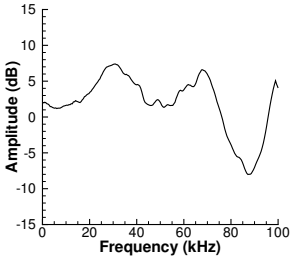

(e) 120°

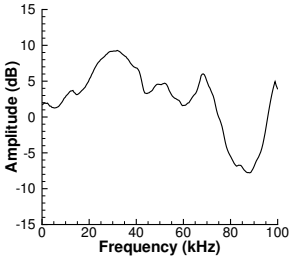

(f) 150°

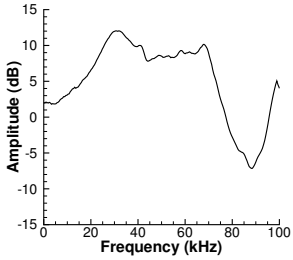

(g) 180°

Figure 29: Correction as of March 2014 for the FITE0009 AMF.

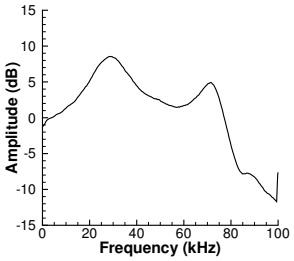

(a) 0°

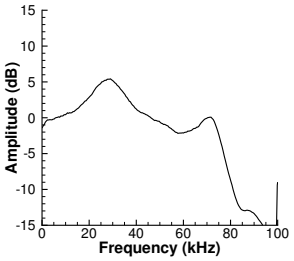

(b) 30°

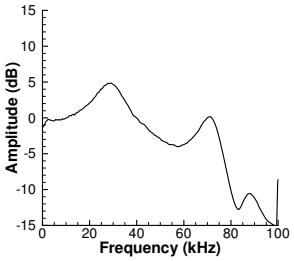

(c) 60°

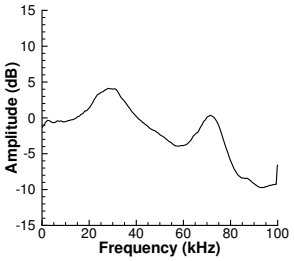

(d) 90°

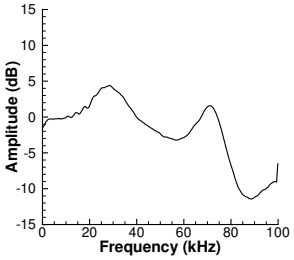

(e) 120°

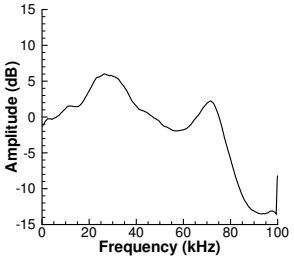

(f) 150°

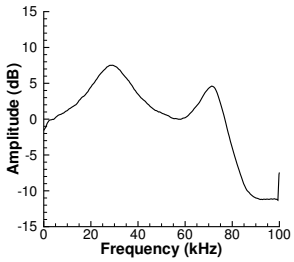

(g) 180°

Figure 30: Correction as of March 2014 for the FITE0010 AMF.

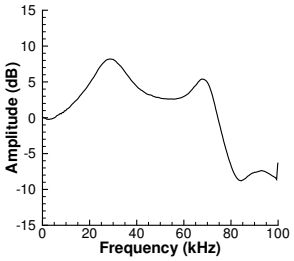

(a) 0°

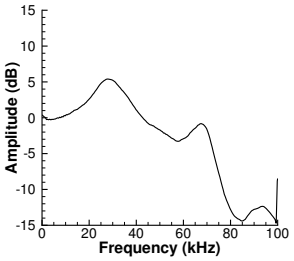

(b) 30°

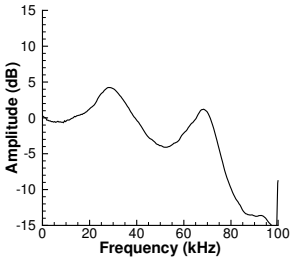

(c) 60°

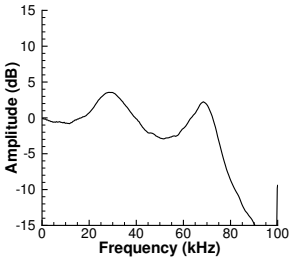

(d) 90°

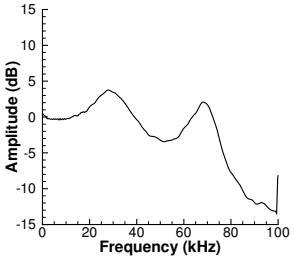

(e) 120°

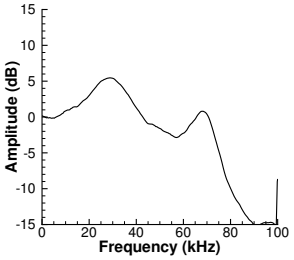

(f) 150°

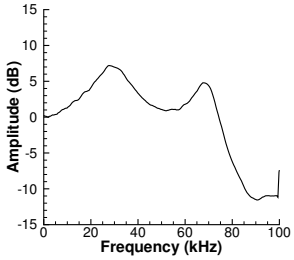

(g) 180°

Figure 31: Correction as of March 2014 for the FITE0011 AMF.

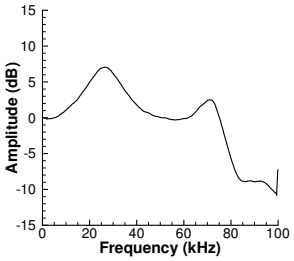

(a) 0°

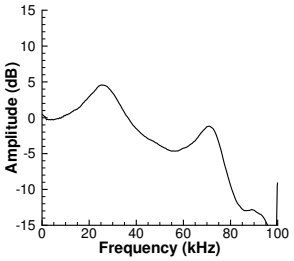

(b) 30°

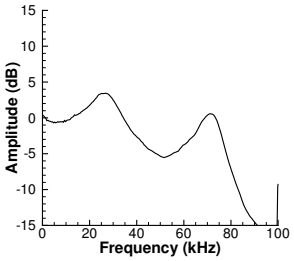

(c) 60°

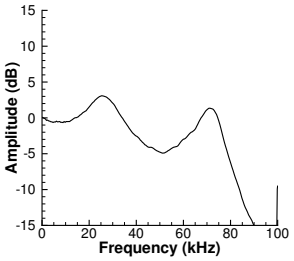

(d) 90°

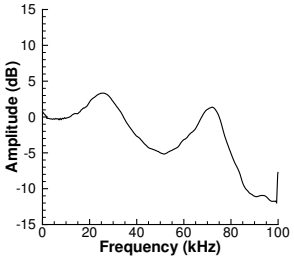

(e) 120°

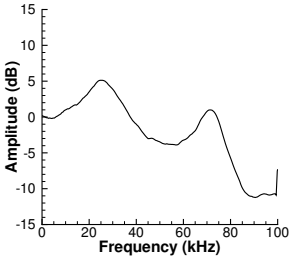

(f) 150°

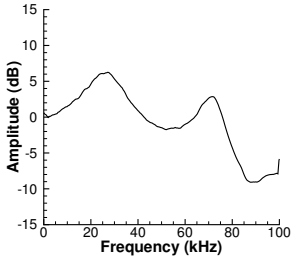

(g) 180°

Figure 32: Correction as of March 2014 for the FITE0012 AMF.

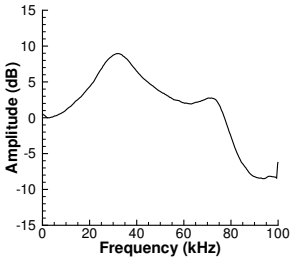

(a) 0°

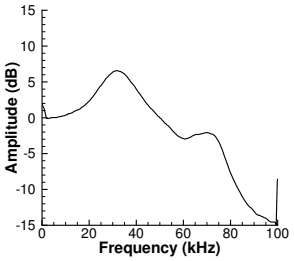

(b) 30°

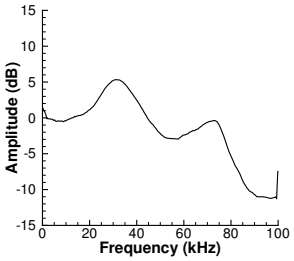

(c) 60°

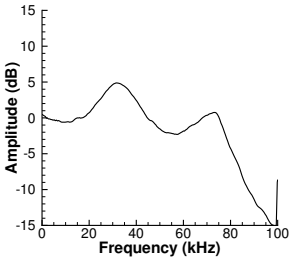

(d) 90°

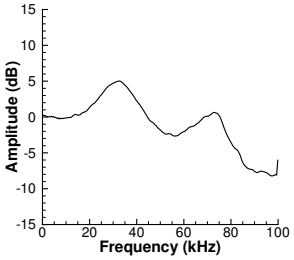

(e) 120°

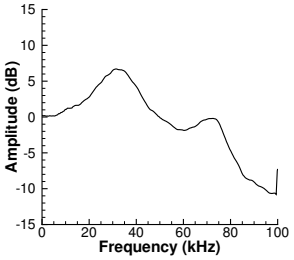

(f) 150°

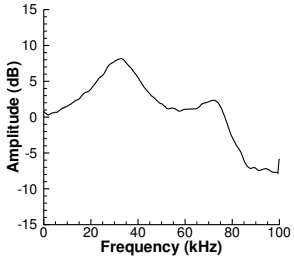

(g) 180°

Figure 33: Correction as of March 2014 for the FITE0013 AMF.

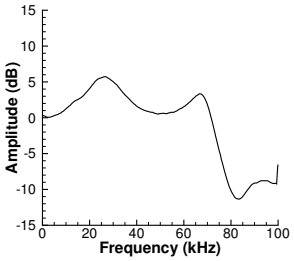

(a) 0°

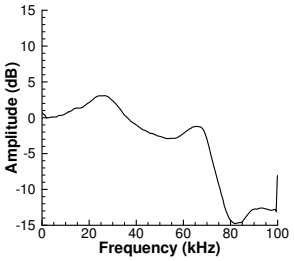

(b) 30°

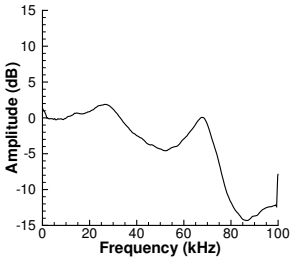

(c) 60°

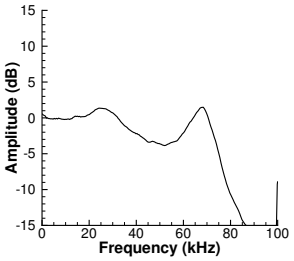

(d) 90°

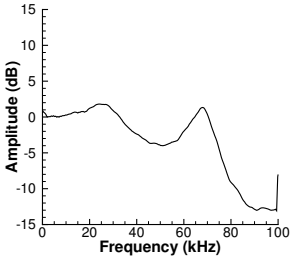

(e) 120°

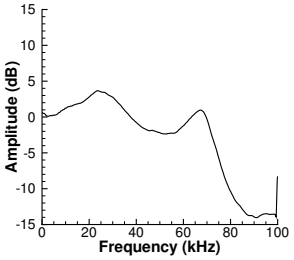

(f) 150°

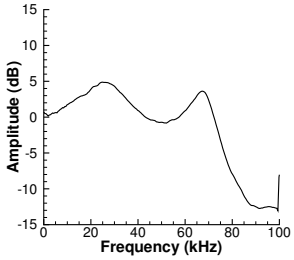

(g) 180°

Figure 34: Correction as of March 2014 for the FITE0014 AMF.

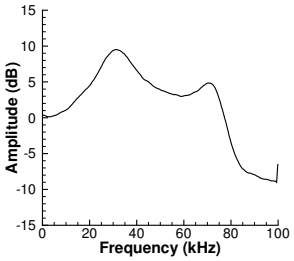

(a) 0°

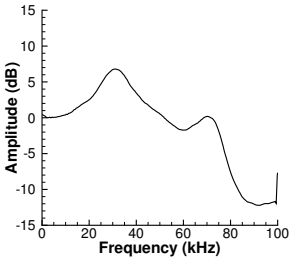

(b) 30°

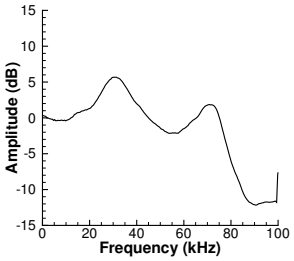

(c) 60°

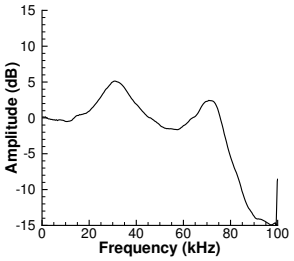

(d) 90°

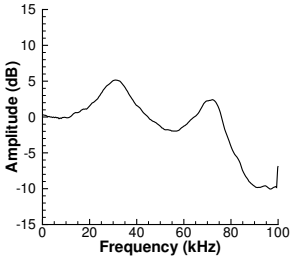

(e) 120°

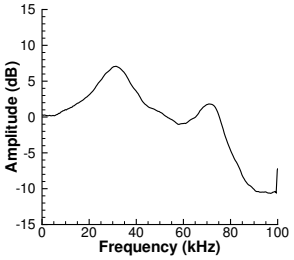

(f) 150°

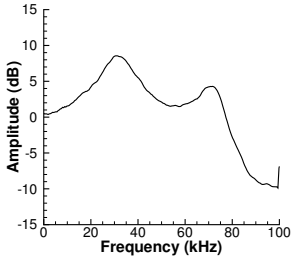

(g) 180°

Figure 35: Correction as of March 2014 for the FITE0015 AMF.

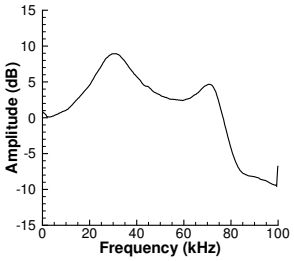

(a) 0°

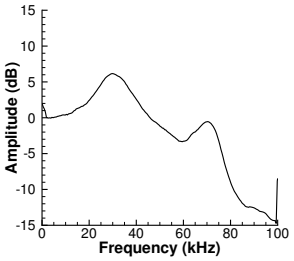

(b) 30°

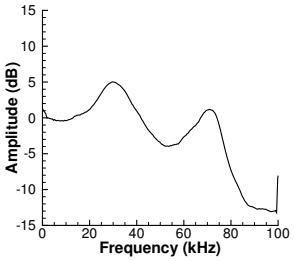

(c) 60°

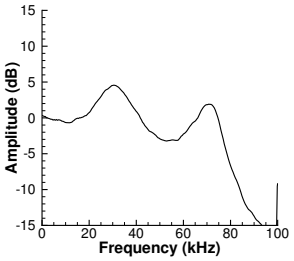

(d) 90°

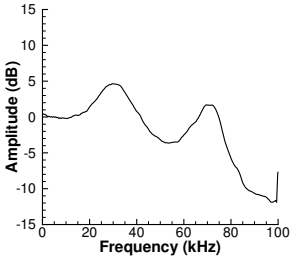

(e) 120°

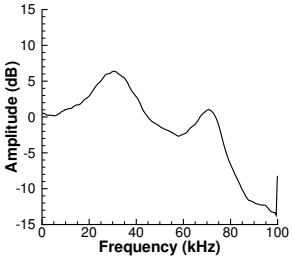

(f) 150°

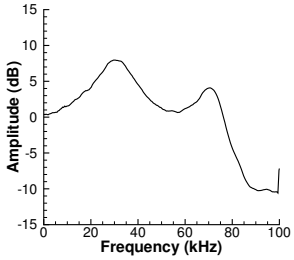

(g) 180°

Figure 36: Correction as of March 2014 for the FITE0016 AMF.

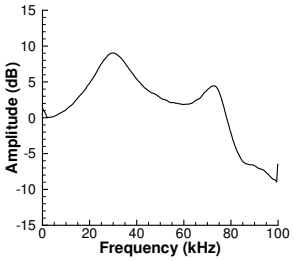

(a) 0°

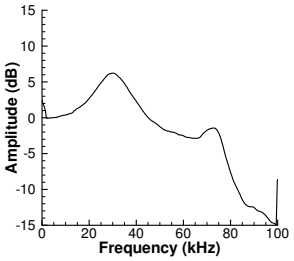

(b) 30°

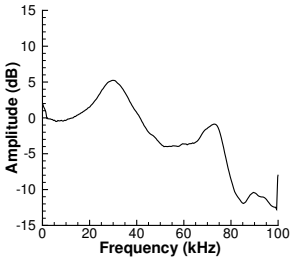

(c) 60°

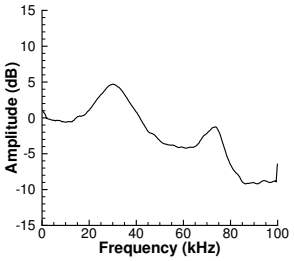

(d) 90°

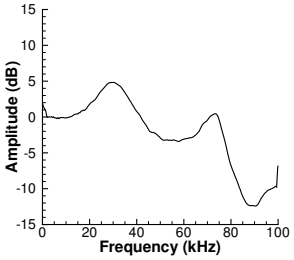

(e) 120°

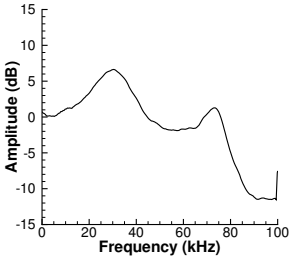

(f) 150°

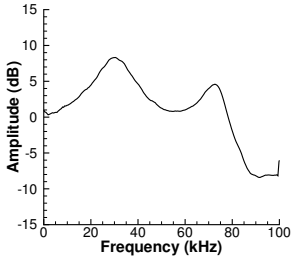

(g) 180°

Figure 37: Correction as of March 2014 for the FITE0017 AMF.

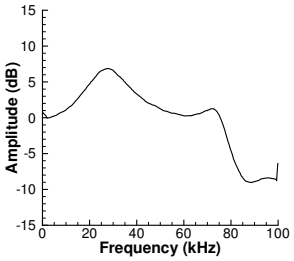

(a) 0°

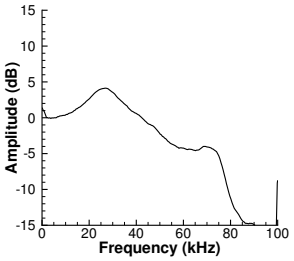

(b) 30°

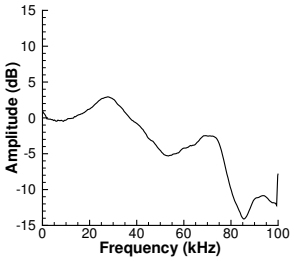

(c) 60°

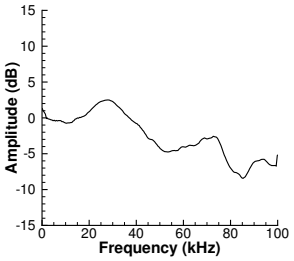

(d) 90°

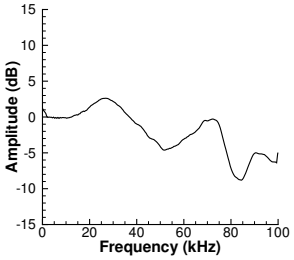

(e) 120°

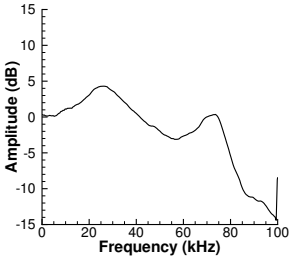

(f) 150°

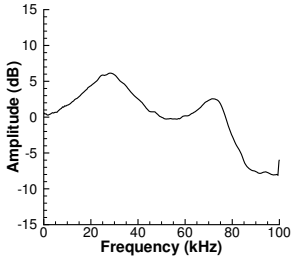

(g) 180°

Figure 38: Correction as of March 2014 for the FITE0018 AMF.